THESIS

INTERACTION OF $[VO_2(MA)_2]^-$ WITH MODEL MEMBRANES: RELEVANCE TO INSULIN ENHANCING EFFECTS OF BMOV AND ITS OXIDIZED FORM

Submitted by

Samantha Kay Schoeberl

Department of Biomedical Science

In partial fulfillment of the requirements

For the Degree of Master of Science

Colorado State University

Fort Collins, Colorado

Summer 2010

COLORADO STATE UNIVERSITY

JUNE 24, 2010

WE HEREBY RECOMMEND THAT THE THESIS PREPARED UNDER OUR SUPERVISION BY SAMANTHA KAY SCHOEBERL ENTITLED INTERACTION OF $[VO_2(MA)_2]^-$ WITH MODEL MEMBRANES: RELEVANCE TO INSULIN ENHANCING EFFECTS OF BMOV AND ITS OXIDIZED FORM BE ACCEPTED AS FULFILLING IN PART REQUIREMENTS FOR THE DEGREE OF MASTER OF SCIENCE.

Committee on Graduate Work

James Graham

Debbie Crans

Advisor: Deborah Roess

Department Head: Colin Clay

ABSTRACT OF THESIS

INTERACTION OF $[VO_2(MA)_2]^-$ WITH MODEL MEMBRANES: RELEVANCE TO INSULIN ENHANCING EFFECTS OF BMOV AND ITS OXIDIZED FORM

Anti-diabetic vanadium-containing compounds and salts reportedly have effects on the overall organization of the cytoskeleton and the plasma membrane of cells. For ligand-mediated signaling, appropriate cytoskeletal and membrane lipid organization is essential for down-stream signaling to occur. A number of vanadium-containing compounds and salts are of interest because of their effects on these important cellular structures. Promising results in regulating diabetic symptoms such as glucose and lipid metabolism have been shown to result from the use of various anti-diabetic vanadium drugs. Their effects on the cytoskeleton and plasma membrane are reviewed Chapter I.

Due to the importance of membrane interactions of vanadium-containing compounds with insulin-enhancing activity in ligand-mediated signaling, two simple membrane model systems were used to investigate the interactions of an oxidized metabolite of bis(maltolato)oxovanadium(IV) with model lipid interfaces. Studies were carried out using multinuclear NMR spectroscopy with a focus on ^1H NMR techniques. In Chapter II we demonstrate that there were slight changes in ^1H NMR spectra indicating that this BMOV metabolite was able to penetrate the lipid interface. These

findings are important in understanding the pharmacologic mechanism of action of this anti-diabetic compound in cells and intact animals.

Samantha Kay Schoeberl
Department of Biomedical Science
Colorado State University
Fort Collins, CO 80523
Summer 2010

ACKNOWLEDGMENTS

I would like to begin by thanking all of the members on my thesis committee including Dr. James Graham, Dr. Debbie Crans and Dr. Deborah Roess. I would like to give a special thank you to Drs. Crans, Roess and Willsky for being supportive, providing constructive feedback and for encouraging me to pursue my goals and dreams. What a delight and an honor to have been able to work with you both. I also want to thank the members of Dr. Roess' and Dr. Barisas' research group for their suggestions when needed. A very much deserved "thank you" is due to all of the members of Dr. Crans' research group for providing moral support when times became hectic and also setting time aside for exciting discussions about nearly everything. I cannot thank you enough and each one of you will be truly missed. Another thank you must go to the CIF and the analytical specialists who have taken their time in training me on the NMR. My thesis could not have been successful without their assistance.

My family has also been very supportive and encouraging during my time at CSU and I would like to sincerely thank my family for being there for me. I appreciate them for being endlessly understanding with regard to the importance of my continued education knowing that my time with them was limited as a consequence of pursuing my dreams. I would also like to thank Justin Green for his continuous effort, positive encouragement and support all these years. Thank you.

TABLE OF CONTENTS

LIST OF TABLES

LIST OF FIGURES

CHAPTER I[1]

EXAMINING INTERACTIONS OF VANADIUM COMPOUNDS WITH CELL CYTOSKELETON, CELL MEMBRANES AND WITH MODEL MEMBRANES

INTRODUCTION

Vanadium-containing complexes and vanadium salts represent a unique class of compounds that have been used to study cell functions including phosphatase activity during signal transduction and mechanisms involved in insulin-mediated signaling. Selected compounds have also been evaluated as pharmacologic agents for treatment of diabetes (1-14). Because of their broad utility as biologic agents, there have been numerous reviews of vanadium derivatives (1, 2) and their chemistry (3-8, 13, 15), the insulin-enhancing properties of vanadium-containing compounds that include effects on diabetic hyperglycemia and hyperlipidemia (9-11), and the mechanism of action for vanadium salts in either +4 or +5 oxidation states in *in vivo* and *in vitro* systems (11, 12, 14, 16, 17). Here we will focus on some less considered aspects of vanadium's

---

[1] This chapter is currently being prepared as a review article entitled "Do plasma membrane and cytoskeletal components play a role in the modulation of signal transduction by vanadium compounds? Examining interactions of vanadium compounds with cell cytoskeleton, cell membranes, and with model membranes". The authors of this review are: Samantha K. Schoeberl, Debbie C. Crans, Gail R. Willsky, and Deborah A. Roess.

physiologic functions. These include effects of vanadium compounds on the plasma membrane and cytoskeleton that lead to modification of ligand-initiated signal transduction. We will also discuss the use of model systems for evaluating interactions between vanadium-containing compounds or salts with biologically-relevant membrane proteins and lipids.

CHEMICAL PROPERTIES OF BIOLOGICALLY-RELEVANT VANADIUM COMPOUNDS OR SALTS

A range of vanadium complexes and salts have been used in studies examining vanadium's effects on the cell membrane and the cytoskeleton. The aqueous chemistry of vanadium is highly complex and includes protonation, oligomerization and redox chemistry, and has been described extensively (6). Commonly used biologically-active forms of vanadium include decavanadate, vanadyl and vanadate salts, as well as vanadium complexes with varying ligands.

Vanadium Salts

Most biological studies have used vanadium(V) in the form of vanadates containing sodium salt or, in earlier studies, ammonium salt, or vanadium(IV) in the form of vanadyl sulfate (see Figure 1 for vanadate and vanadyl salt formations). Like decavanadate, the vanadium(IV) salt, vanadyl sulfate (Figure 1b), has complex aqueous chemistry (6). The vanadium(IV) compound is not redox stable in the presence of oxygen at neutral pH and undergoes oligomerization and polymerization reactions in the absence of chelating agents. Chelating agents are also necessary for improving

absorption of vanadium salts from the gastrointestinal tract (18) and, once absorbed, vanadium salts have insulin-enhancing effects by controlling glucose regulation (2, 19).

Decavanadate

Vanadate in its simplest form is a phosphate analog, structurally and electronically (20). Vanadate oligomer formation is dependent upon the pH of the solution and its concentration. The colorless vanadate dimer resembles pyrophosphate structurally and electronically. At physiological pH (6.8-7.2), oligomer forms of vanadate are evident. For example, at low concentration (1.25 mM) the main oligomers present are tetra- and monomeric vanadate along with small amounts of di- and pentameric vanadate. At high concentrations (40 mM), tetra- and pentavanadates are the main species observed while monomers and dimers are present in negligibly small amounts.

One specific oligomeric vanadate whose chemistry and biology has been extensively studied is decavandate (Figure 1a) (21). Decavanadate is a highly charged hexa-anion at neutral pH, a compact polyvanadate containing ten vanadium(V) atoms with geometric dimensions of 5.4 x 7.7 x 8.3 Å (22, 23), and readily forms over a pH range of 3-6. More alkaline conditions will, however, cause decavanadate fragmentation into phosphatase-inhibiting vanadate monomers and oligomers (21). Thus, reports suggesting that decavanadate is a phosphatase inhibitor should include studies with vanadate monomer which demonstrate that inhibition is not simply the result of decavanadate but could be due to decomposition into vanadate monomers (21).

Vanadium Coordination Complexes

Coordination complexes that have been used in studies of cell membranes and the cytoskeleton are shown in Figure 2. In order to study the chemistry of these compounds in solution or their location in simple model systems, vanadium in the +4 and +5 oxidation states are studied by EPR and NMR spectroscopy, respectively. The chemistry of these complexes is well described elsewhere (24, 25) and, in general, the vanadium(IV) complexes are more stable than the vanadium(V) and (III) complexes in the reducing cellular environments. However, vanadium(V) complexes function as insulin-enhancing agents (15, 16, 26) with greater efficacy than vanadium(IV) complexes (19).

A GENERAL SURVEY OF PHYSIOLOGIC EFFECTS OF VANADIUM COMPOUNDS

Vanadium derivatives are known to affect cell function in a variety of ways. Most work with vanadium-containing compounds has examined effects on phosphatase activity, insulin-like activity in biochemical assays, and effects on gene expression in diabetic animal models. *In vivo* and *in vitro* cellular effects have been extensively reviewed (1, 6, 10, 11, 15, 27-30) and are summarized below.

Phosphatase Inhibition

Vanadium-containing compounds and salts including simple vanadium salts (31, 32), peroxovanadium (33, 34), vanadium(IV) (35), vanadium(V) (34, 36), BMOV (37), $VO(pa)_2$ (38), a derivative of VO_2(dipic) specifically VO_2(dipic-NH_2) (39), and other

vanadium derivatives with natural product ligands have been shown to inhibit a variety of phosphatases including tyrosine (32, 40-43), and glucose-6 phosphatases (37) that are also up-regulated in diabetic insulin signaling pathways (44). It is also worth noting that enzyme solution studies are complicated by the fact that experimental conditions used to optimize enzyme activity can be less than optimal for compound stability. As a result, observed effects of vanadium complexes may ultimately be attributed to vanadate or vanadyl cation alone because assay conditions, i.e., the type of buffer or compound concentration, have the potential to cause complex-ligand dissociation and may result in inaccurate interpretation of complex activity (6, 34, 45).

Insulin-Enhancing Vanadium Compounds

Vanadium-containing compounds and vanadium salts have been explored for use in treating Type I and Type II diabetes. It was soon recognized that vanadium treatment did not completely replace insulin in insulin-dependent animal models such as the inbred BioBreeding (BB) rat model for Type 1 diabetes in humans, and was briefly commented on in a review by Cam and colleagues (17). Because some insulin must be present for vanadium to be effective, it is now generally accepted that vanadium compounds function as insulin-enhancing agents.

The detailed mechanism by which insulin action is enhanced by vanadium compounds remains unresolved. Insulin functions via a hormone-specific plasma membrane receptor that, upon binding insulin, undergoes autophosphorylation. This pivotal event, through intermediate signaling molecules, then leads to activation of PI-3K (44) and activation of further downstream signaling molecules. Vanadium-containing

compounds appear to act selectively on enzymes downstream in the insulin signaling cascade, specifically targeting protein phosphatases (39, 42, 46-49). Because complications of Type II diabetes are often associated with the insulin receptor's inability to undergo autophosphorylation, one possible target of vanadium compounds is tyrosine phosphatase 1B which specifically dephopshorylates the insulin receptor (50).

Vanadium-containing compounds normalize glucose metabolism, lipid metabolism, and cholesterol levels in addition to other insulin-enhancing activities. Any or all of these effects may result from inhibition of phosphatase activity (19). Vanadium(V) complexes been extensively investigated for insulin-enhancing activity (15, 16, 26). These compounds may be more efficacious than vanadium(IV) compounds (19) which, nonetheless, are more stable than the vanadium(V) and (III) complexes in reducing cell environments. The chemistry of these complexes is well described elsewhere (24, 25). In animal models of diabetes, vanadium(III) complexes with various maltol-related (19) or dipicolinate ligands (51) have been reported to be stable and effective at normalizing blood glucose levels in STZ diabetic rats (19, 51). *In vivo*, vanadium complexes with (IV) and (V) oxidation states along with vanadium salts decrease blood glucose and lipid levels in diabetic rats (52) while vanadium salts normalize diabetic hyperglycemia (53) and enhance insulin sensitivity (53).

Effects of Vanadium Compounds on Gene Expression

Vanadium treatment has marked effects on a wide range of cellular functions including metabolism, transport, and cytoskeletal remodeling. Long-term exposure to vanadium compounds also affects gene expression by either down regulating (37, 54-59)

or up-regulating genes that are impacted in diabetic rat models (54, 55 633, 56, 59). More specifically, various vanadium compounds have been shown to down regulate cytoskeletal gene expression (Table 1), membranes and transporters involved in carbohydrate metabolism/transport (Table 2), membranes and transporters involved in lipid transport/metabolism (Table 3), and down regulate gene expression of the insulin receptor (Table 4). In STZ-induced diabetic animals, oral administration of vanadium salts ($VOSO_4$ and $NaVO_3$) and vanadium complexes, such as BMOV and $VO(alx)_2$ results in various transcriptional effects (37, 54-59). In most studies, vanadium treatment decreased expression of genes as summarized in Tables 1-5. However, a few genes are expressed at higher levels in diabetic animals (summarized in Table 5) and these are associated with carbohydrate and lipid metabolism/transport. Vanadium derivatives have also displayed an effect at the genomic level where vanadate has been shown to alter the expression of essential enzymes in the liver and kidney that are required for gluconeogenesis, specifically PEPCK (56, 60).

Vanadate has also been used in diabetic rat models to demonstrate normalization of ketone levels in rats experiencing ketoacidosis (56). Ketoacidosis is a complication seen most frequently in Type 1 diabetes mellitus but can occur in patients with Type 2 diabetes as well. When there is not enough intracellular glucose for cellular metabolism, fat stores are used as an energy source. Diabetic ketoacidosis results when ketones, produced in large amounts during fat metabolism, appear in higher levels in the circulation and cause a decrease in blood pH. HMGCoAS is a regulatory enzyme involved in the production of ketones in the liver and vanadate blocks the up-regulation of this gene (56).

VANADIUM EFFECTS ON THE CYTOSKELETON

The cytoskeleton provides architectural structures that maintain the three-dimensional shape of a cell, function in cell mobility, support cell organelles, and assist in the transport of membrane components to and from the plasma membrane. The cytoskeleton is composed of three major structural components; microtubules, intermediate filaments, and microfilaments, each of which can be independently affected by vanadium derivatives.

Microfilaments and Vanadium Compounds

It has been suggested that vanadium toxicity may be a result of interactions with actin microfilaments (21, 61-64). Microfilaments provide structural support for the cell, are involved in cell locomotion, and organize cellular components during cytokinesis (65). Microfilaments are found in the cytoplasm and have dynamic organization, assembling and dissembling quickly. Nucleation, the intial step in the formation of filamentous actin (F-actin) from actin subunits, involves polymerization of globular actin (G-actin) subunits. There is a lag phase between nucleation and elongation; the time required for progression from nucleation to elongation is dependent upon the concentration of monomeric actin within the cell. Once nucleation is complete, microfilaments elongate unidirectionally due to molecular polarity with polymerization using ATP·G-actin occurring at the positive end of the microfilament structure. Filament elongation continues until equilibrium is reached between the monomer assembly rate and disassembly rate which occurs at a critical concentration C_c. Actin assembly and disassembly is discussed in more detail in the following sources (65-68).

Vanadium(V) Effects on Microfilaments

Orthovanadate ($NaVO_4$) and metavanadate ($NaVO_3$) are frequently used V(V) salts in studies of the effects of vanadium on microfilaments. Since the interconversion of one to the other is pH and concentration dependent, the form of the V salt present at a given concentration is solely dictated by the solution in which the experiments are performed. We will refer to orthovanadate and metavanadate only to indicate which form was originally used in the experiment. Other forms of vanadium(V) include decavanadate and vanadium(V) coordination complexes.

Vanadate

The addition of orthovanadate has been shown to stabilize F-actin at low concentrations prepared from rabbit skeletal muscle (64), presumably as a result of its structural homology with P_i and binding affinity. However, addition of 2 mM of metavanadate to actin had no effect on the structural organization of the microfilaments from rabbit skeletal muscle that actin was extracted from (62). However, in Caco-2 cell lines, 1 mM of $NaVO_3$ promoted actin condensation (61). These results show that the effects of vanadate on microfilaments are dependent upon the biological cell line used for the experiment although the concentration of the salt may also be important.

Decavanadate

Decavanadate has been recently shown to enhance the uptake of glucose in adipose tissue (69). Although this is beneficial to diabetic patients, decavanadate at high concentrations has been shown to affect cytoskeletal organization by preventing G-actin

polymerization (21, 62) as do vanadates (70). Decavanadate has been shown to inhibit the rate of G-actin polymerization by half at approximately 68 μM and inhibit the elongation of microfilaments at 17 μM of decavanadate (62). Using ^{51}V-NMR spectroscopy, Ramos and colleagues demonstrated that decavanadate was stabilized upon addition of G-actin and its half-life increased 5-fold over that without G-actin. ATP destabilizes decavanadate by decreasing its half-life from 27 to 10 hours in a G-actin/decavanadate/ATP solution (62). Since ATP binds to G-actin to enable filamentous structure assembly, ATP may have a greater affinity for G-actin than decavanadate which suggests why decavanadate is unstable upon ATP addition.

It has been suggested that because decavanadate inhibits G-actin polymerization, its effects result from interactions with the ATP-binding site on the G-actin monomer. Since orthovanadate maintains the filament structure due to V_1 similarities to phosphate by maintaining the F-actin-ADP + V_1 structure (64) one would predict that, if ATP is not able to bind G-actin, polymerization to a filamentous structure should decrease. These studies have not, however, been performed. Nevertheless, it appears that upon the addition of decavanadate to G-actin, polymerization does not occur and decavanadate becomes stabilized. Figure 3 illustrates actin polymerization with ATP hydrolysis and also shows a potential mechanism for how decavanadate and its derivatives may prevent this polymerization from occurring and how V_1 actions may promote polymerization.

In addition to cytoskeletal function, actin filaments, together with myosin (myosin-II) form the molecular apparatus in muscle cells used in muscle contraction. For muscle contraction, ATP hydrolysis occurs quickly where myosin ATPases must act on the myosin-subfragment 1 (myosin-S1) substrate in order for the myosin-S1 to bind to

actin. Once the P_i is released, the myosin head moves the actin filament along the myosin creating a power-stroke movement, a process then repeats itself as long as ATP is available. Studies from the early 1980's showed that ATPase activity was inhibited significantly by binding of vanadate to form an ADP-V-myosin complex (71). Decavanadate also prevented F-actin from stimulating the ATPase activity on the subfragment-1 complex on myosin. Additionally, sodium vanadate promoted actin polymerization by forming an F-actin-ADP-V_1 complex that enabled filament stabilization (21, 61, 70). At concentrations of 50 μM of V_{10}, decavanadate strongly inhibited this activity at a concentration of approximately 0.8 μM (63, 642). The interactions of decavanadate with microfilaments were the most potent of any vanadium compound described in this review.

Vanadium-Semicarbazone Complexes (V(V)-Salsem)

The cytotoxicity of vanadium-semicarbazone complexes (V(V)-Salsem) was examined in osteoblast MC3T3-E1 and osteosarcoma UMR-106 cells lines. V(V)-Salsem altered cell morphology by disrupting actin in the cytoskeleton framework leading to morphological changes to the plasma membrane. These effects became more dramatic at high concentrations of the vanadium-containing complex; cell shape was altered and rearrangement of actin was observed at 100 μM of V(V)-Salsem although treating osteosarcoma cells with 25 μM V(V)-Salsem produced detectible effects. At 100 μM, some cell nuclei disintegrated as did the plasma membrane (72).

Vanadium(IV) Effects on Microfilaments

A number of vanadium derivatives, particularly vanadyl acetylacetonate ($VO(acac)_2$), bis(maltolato)oxovanadium(IV) (BMOV or $VO(ma)_2$), in addition to vanadate have been shown to have an effect on actin filaments where microvilli became less organized upon addition of 1 mM of $VO(acac)_2$. Comparison of these vanadium derivatives and their cytoskeletal effects was also examined on the Caco-2 cells in which actin filaments were fluorescently labeled using rhodamine-phalloidin. Vanadate (1 mM) caused a greater alteration in the filament structure and actin condensation than did $VO(acac)_2$ and $VO(ma)_2$ supporting the notion that vanadium complexes utilize the ATP-binding site on actin and inhibit microfilament formation (61). As with the V(V) vanadate these experiments with V(V) compounds indicate that the concentration of the vanadium compound administered play a major role in actin reorganization. These results could be explained if actin filaments were a site for vanadium to bind (61).

Vanadium(III) Effects on Microfilaments

A small number of studies have investigated the effects of vanadium(III) on actin filaments in hepatoma Morris 5123 cells. Low concentrations of vanadium(III) promoted rearrangement of actin filaments to form focal sites in the cell as compared to the more uniform cytoplasmic distribution of actin filaments in the absence of vanadium(III) (73). Highly concentrated areas of actin were found near the nucleus and the plasma membrane after vanadium(III) addition and plasma membrane blebbing was also observed as the V(III) concentration increased; the most dramatic changes in cells were detected at 100 μM of V(III) (73).

Intermediate Filaments and Vanadium

Intermediate filaments (IF), which range in diameter from 10-12 nm (74), are located within the cytoplasm and nuclear envelope where they provide structural support for the nucleus and other organelles, and form desmosome adhesions between cells (75). They are comprised of specific proteins, do not require ATP hydrolysis for assembly, and have cell-specific expression including, as examples, keratins in skin and hair cells, lamins in the nuclear lamina, and vimentins in muscle cells. There are six different types of IFs and the proteins that comprise these filaments are associated with over 30 diseases including dermatologic diseases, hepatic cirrhosis, and inflammatory bowel disease. Effects of mutations in intermediate filament genes on disease processes have been reviewed recently (74, 76).

A small number of studies have examined vanadium derivatives and their impact on IF formation. Orthovanadate treatment prevents complete framework formation of keratin intermediate filaments (75) and enhances keratin granule formation. This may occur through orthovanadate-mediated effects on phosphorylation of p38 which promoted additional keratin granule formation and phosphorylation (77). Interestingly, Strnad and colleagues treated epithelial cells for 1-10 minutes of light and found that the keratin microfilaments became resistant to orthovanadate (75).

Vanadium-Microtubule Interactions

Microtubules, approximately 25 nm diameter (78), are hollow tubular structures composed of alpha-beta tubulin heterodimer subunits. They form part of the cytoskeleton in eukaryotic cells, provide support for cells experiencing tensile stress, and are critical

for chromosome separation during mitosis. Kirazov and Weiss have shown that there is concentration-dependent vanadate inhibition of microtubule protein (MTP) assembly (79). MTP assembly was inhibited by 12% at 100 μM and by 65% at 700 μM vanadate concentrations that, however, did not alter structural features of MTPs (79).

VANADIUM EFFECTS ON PLASMA MEMBRANE PROTEINS

Membrane proteins are responsible for the majority of membrane-mediated cellular processes. Among other functions, they act as ligand-specific receptors, facilitate diffusion of ions and small molecules across the membrane, serve as ion channels and provide active transport of selected ions. Vanadium compounds and salts have been shown to have an effect on membrane protein functions as well as alter the organization of membrane proteins in the lipid bilayer. Although vanadium can inhibit many membrane-bound proteins by binding at the active site, many effects of vanadium-containing compounds or vanadium salts on cell membrane proteins are indirect. Introduction of vanadium either alters some aspect of cellular function that, in turn, alters membrane protein function. Alternatively, vanadium modify membrane lipid packing that impact the distribution of membrane proteins in plasma membrane microdomains. The change in the local lipid environment can alter protein function. This section describes vanadium effects on the activity of four representative membrane proteins: P-type ATPases, the insulin receptor, a glucose transport protein and the transferrin/transferrin receptor, a metal transporting system.

P-Type ATPases

The P-type ATPases are membrane ATPases or ion pumps for which vanadate functions as a transition state analogue where the terminal phosphate of ATP is attached to the protein via an aspartate residue (80). These membrane ion pumps all utilize the energy from the hydrolysis of ATP to pump various ions across the plasma membrane against their concentration gradient. Most P-type ATPases are located in the plasma membrane while some of them are found in intracellular membranes such as the calcium pump of muscle cells located in the sarcoplasmic reticulum membrane. They have been characterized into three groups by a comparison of the structural diversity and the type of cation transported (81). In this classification the Na^+, K^+ ATPase, Ca^{++} ATPase, and H^+ ATPases are part of the P2 class involving the transport of ions that are not heavy metals. In a later analysis based on a molecular biology study of the evolution of the substrate specificity (82) these ATPases are divided into five evolutionary branches which are: Ca^{2+} ATPase, Na^+, K^+ ATPase and H^+, K^+ ATPase in type II and the H^+ Mg^+ ATPases in an evolutionarily divergent type III.

The effects of lipid variation on the activity of the plant plasma membrane H^+ ATPase has been well studied (83). This enzyme requires lipids for activity and it has been suggested that modification of the lipid environment by changes in fluidity or lipid composition could change the activity of the enzyme. With regard to proton pumping, the boundary lipid theory in which certain lipids in an annulus around the protein have the largest effect on activity was favored, rather than the bulk lipid theory in which the enzyme activity is mostly regulated by the changes in the bulk lipid composition.

The effects of lipid modifications on the activity of the sarcoplasmic reticulum calcium pump have been studied since the 1980's. Increasing membrane fluidity caused increased activity while decreasing membrane fluidity inhibited the activity (84). The inhibition of this pump by melittin, a 26 residue peptide, was caused by direct binding of melittin to the membrane lipids as measured by ESR (84).

In order to examine the effects of the specific annulus of lipid surrounding the P-type ATPases and effects of the bulk fluidity properties specific photolabeling probes have been designed. This procedure is more sensitive than the ESR analysis and was tested in the plasma membrane and sarcoplasmic reticulum calcium pump along with the Na^+, K^+ ATPase. The two Ca^{2+} ATPases had similar amounts of molPC/mol protein. The alpha subunit of the Na^+, K^+ ATPase had more lipid bound per protein, while the beta subunit displayed much less lipid bound per subunit than the calcium pumps. The use of a photoactivatable phospholipid probe of the sarcoplasmic reticulum and plasma membrane calcium pumps demonstrate that there are two different E1 conformations of the enzymes, one that is auto-inhibited and has contact with more lipids, while the other one is always active and shows a more compact transmembrane structure (85).

In detailed kinetic analysis of enzyme activity, ion movement and formation of phosphoprotein products after the modification of specific residues of the P-type ATPases there is evidence that E2 conformation effects modifying both activity and V binding occur. This has been shown for the conserved Thr 214 in Domain A of the Na^+, Ka^+ ATPase (86) and with the Asp 706 and Glu 183 in the catalytic site of the Ca^{++} ATPase in the sarcoplasmic reticulum (87). These experiments demonstrate that the

activity of P-type ATPases are directly related to conformational changes in the protein induced by modifications of the active site.

These results that the activity and structure of the P-type ATPases are altered by changes in the lipid environment imply that there may be more vanadium influence on activity in addition to binding at the active site of the ATPases. Vanadium addition to plasma membranes could modify the activity of these enzymes by changing properties of the membrane lipids causing significant conformational changes to occur in the enzyme.

Insulin Receptors

Despite insulin-like activity by selected vanadium-containing compounds, there is little evidence suggesting a direct effect of most vanadium compounds on insulin binding to its receptor. Although we have shown that binding of insulin is not affected by the presence of BMOV (P. Winter et al., manuscript in preparation), Kwong et al. (88) evaluated effects of a panel of peroxovanadates on insulin binding to placental membrane insulin receptors and identified effects of some peroxovanadium compounds on high affinity, low capacity insulin binding sites. Interestingly, compound-specific increases or decreases in insulin binding required a membrane environment.

Longer exposure to vanadium compounds has also been reported to affect the total number of insulin receptors expressed by cells. A V(IV) complex, $VO(saltris)_2$, increases insulin receptor numbers in the plasma membrane in RBL-2 H3 cell as well as activating downstream signaling proteins associated with insulin-mediated signaling (34, 89, 90).

GLUT4 Transporters

Insulin-mediated signaling leads to insertion of the GLUT4 transporter in the plasma membrane of muscle and fat cells. This transporter is responsible for facilitated diffusion of glucose into cells where phosphorylation of glucose helps to maintain the glucose concentration gradient. Oxovanadium and vanadyl derivatives (91, 92) have been shown to enhance the translocation of GLUT4 proteins from intracellular compartments to the plasma membrane cellular systems as have other vanadium-containing compounds (91, 93-95). In 3T3-L1 adipocytes, GLUT4 receptors were tracked using immunofluorescence staining as they progressed through the cell in response to $VO(alx)_2$ or $VOSO_4$. While translocation of GLUT4 to the membrane was observed upon addition of either 50 nM insulin or 50 μM $VO(alx)_2$, 50 μM $VOSO_4$ was less effective (93).

Transferrin and Transferrin Receptors

Transferrin and its receptors participate in iron transport in the blood and uptake of iron by cells expressing the transferrin receptor. More recently, there have been reports of vanadium transport by transferrin suggestive of interactions between vanadium and transferrin (96-98). Although this issue has not been resolved, vanadium derivatives in the blood dissociate into their ions and it appears that these vanadium ions interact with transferrin. Two vanadyl ions have been shown to bind to the iron binding sites on the transferrin protein due to the stronger chelating properties of transferrin compared to maltol ligands. Willsky and colleagues used EPR methods to evaluate interactions between BMOV and $VOSO_4$ with human apotransferrin and showed that vanadyl ions

from BMOV and $VOSO_4$ were the interacting species (97). Liborion et al. showed preferential binding of vanadyl ions from $VOSO_4$ and BMOV bind in the Fe(III) sites on the serum transferrin protein subunit following breakdown of BMOV to vanadyl ions (96) and suggested that transferrin was providing vanadyl ion transport *in vivo*. Similarly, in rat adipocytes, vanadate has been shown to be bound to transferrin (98).

Effects of vanadium-containing compounds and salts on the transferrin receptor are due to either transferrin receptor localization to the plasma membrane, effects on transferrin receptor expression, or transferrin receptor transport to the plasma membrane. Addition of vanadate to adipocytes increased the number of transferrin receptors which increased receptor binding capacity for transferrin and iron uptake into the adipocytes, an effect similar to that of insulin on iron transport (98). There are also suggestions that, in response to chronic vanadate exposure, there is a relatively rapid initial decrease in binding capacity but that after eighteen hours, the transferrin receptor binding affinity increases (49). In addition, iron transport by the transferrin receptor is not prevented by vanadate (98).

EFFECTS OF VANADIUM ON MEMBRANE LIPIDS

As described in the Singer-Nicolson model (99), plasma membranes are made up of a lipid bilayer in which contains membrane proteins, glycolipids and glycoproteins. Membrane lipids are a highly diverse group of molecules which, because of their structural differences, tend to form small microdomains that concentrate particular subclasses of lipids. These microdomains have large variations in size and composition and can undergo both, diffusion in the plane of the membrane and reorganization.

One class of microdomains that has received considerable attention are lipid-containing rafts. Lipid rafts have high concentrations of cholesterol, sphingomyelin and glycosylphosphatidylinositol (GPI)-anchored proteins (100-102) relative to the bulk lipid membrane and can have interactions with actin filaments making up the underlying cytoskeleton (103). Rafts are defined biochemically based on the properties of membrane fragments separated based on buoyant density in sucrose gradients. As suggested by their name, raft fragments "float" in these gradients. The higher buoyancy of membrane rafts appears to result from their high cholesterol content; cholesterol contributes to packing of the phospholipids and makes these cholesterol-enriched microdomains resistant to solubilization by cold non-ionic detergents such as Triton X-100. Cholesterol-enriched microdomains can also be contrasted with the "bulk" plasma membrane where phospholipids are more loosely packed and thus more fluid (104). Molecules capable of binding cholesterol, including cyclodextrins (CD), disrupt these microdomains and typically produce a more uniform distribution of raft-associated proteins within the plasma membrane (105).

Rafts may play a fundamental role in the function of some membrane proteins. Rafts can contain high concentrations of membrane proteins necessary for cell signaling such as G-proteins (106) and adenylate cyclase (107), and this has led to the suggestion that these structures serve as signaling platforms in the plasma membrane. This has certainly been the case for insulin-mediated signaling via its receptor which results in the dynamic association of the insulin receptor with these plasma membrane microdomains (108). Thus, it has been clearly shown that raft localization together with insulin-receptor phosphorylation is required for subsequent interactions between the phosphorylated

receptor and downstream signaling molecules. This includes phosphorylation of insulin receptor substrate-1 (IRS-1) which is recruited to the insulin receptor and uptake of glucose via the GLUT4 transporter. If the insulin receptor cannot access functional rafts, insulin binds its receptor but downstream signaling by insulin receptor is compromised. This may be due to disruption of insulin receptor autophosphorylation (108) or uncoupling of the phosphorylated insulin receptor from downstream signaling events including IRS-1 phosphorylation by insulin receptor (109). The importance of raft microdomains can be demonstrated by disrupting rafts by depleting membrane cholesterol or by excluding the insulin receptor from rafts (108).

Rafts have also been implicated in other aspects of insulin receptor function. Müller and coworkers have shown that rafts, in response to glimeperide, one of the sulfonylurea drugs, concentrate a number of GPI-linked molecules involved in signaling. These signaling molecules also redistribute in rafts with low and high cholesterol content following exposure of adipocytes to glimepiride (110) and this hydrophobic interaction has been implicated in glimepiride function. Although glimepiride acts primarily through stimulation of the insulin secretion from pancreatic beta cells through closing an ATP-sensitive potassium channel, it interacts with membranes in a non-saturable fashion (111) and initiates IRS-1 phosphorylation in adipose cells (112) as well a redistribution of downstream signaling molecules localized in raft sub-populations (110). IRS-1 phosphorylation in response to glimepiride is significantly decreased when membrane cholesterol is depleted, implicating membrane rafts in some aspect of glimepiride signaling. Thus, interactions of lipophilic compounds with the plasma membrane may result in initiation of cell signaling by these compounds. In addition, Chamberlain and

Gould (113) suggest the intriguing possibility that membrane rafts may serve as platforms for both insulin signaling and for trafficking of the GLUT4 transporter, thus linking these events in the same membrane micro-environment. Insertion of GLUT4 may require other proteins that are constitutively located in rafts or translocate to rafts upon phosphorylation (114, 115).

Vanadium compounds affect the distribution of insulin receptors in the plasma membrane. We have shown that brief or overnight treatment of RBL-2H3 cells with BMOV or with 100 nM insulin similarly affects the distribution of the insulin receptor in membrane microdomains (Winter et al., manuscript in preparation). The number of insulin receptors found in raft domains increases significantly in experiments using discontinuous sucrose gradient ultracentrifugation methods to separate raft and non-raft membrane fragments and identification of the insulin receptor on Western blots with an anti-insulin receptor antibody. Tracking the motions of individual insulin receptors on living RBL-2H3 cells using quantum dot-tagged antibodies similarly demonstrates that either BMOV or insulin treatment restricts the motions of insulin receptors to small compartments.

The mechanism involved in driving relocation of insulin receptors into membrane rafts is not known. However, increasing hydrophobicity has been shown to enhance the biological activity of vanadium-containing compounds and, as discussed below for model membranes, interactions between hydrophobic vanadium compounds and the plasma membrane seems likely. Like cholesterol, vanadium compounds may alter lipid packing and produce a redistribution of membrane lipids and affect formation or dissociation of microdomains preferred by membrane proteins. Patented vanadium compounds with

alkyl groups containing up to 12 carbons are highly hydrophobic and more effective than vanadium salts (116).

VANADIUM DERIVATIVES INTERACTING IN MEMBRANE MODEL SYSTEMS

Model membranes consisting of one or a few well characterized lipids have been used to evaluate possible interactions with vanadium-containing compounds. These interactions can be between the lipid interfacial region of a microemulsion, or hydrophobic portions of amphipathic lipids such as when a vanadium complex penetrates the lipid interface during passive diffusion into the cell. Several studies have investigated the interaction of vanadium complexes and vanadium salts with lipid interfaces using both natural lipids and synthetic surfactants (117-120) to determine whether compounds with insulin-enhancing properties in animal systems can penetrate lipid interfaces. Model systems investigated included microemulsions comprised of water in oil (reverse micelle) or oil in water (micelle) systems even though more complex systems could also form. Within these microemulsion systems, various vanadium complexes (V(V)-dipic, (E. Gaidamauskas et al., manuscript in review) (117) and BMOV (118 602) as well as vanadium salts (vanadate, vanadyl sulfate) have been investigated (121).

Vanadium Salts and Model Systems

Studies with the simple vanadium salts have been reported mainly in the AOT/organic solvent/H_2O system (121). Generally the vanadates are found in the water pool more or less associated with the interface depending on the size of the reverse micelle and the specific oxovanadate (23, 118). The vanadates are found to be effective

probes for pH because of their protonation reactions and their oligomerization reactions that are very sensitive to pH (23). A range of studies have been carried out with these systems focusing on how they impact the water pool and interact with the lipid interface and the data support the concept that a pH gradient is established with the water pool being more acidic near the membrane surface than in its core.

Combined, these studies show that some vanadium derivatives can readily penetrate the lipid interfaces and diffuse through the membrane. The role of the ligand for these complexes is critical because while the complex can penetrate the membrane, the simple salt in the absence of ligand do no penetrate the lipid interface. Studies carried out with vanadium complexes show that the ligand becomes separated from vanadium upon administration to diabetic animals (144). However, prior to separation from the ligand the vanadium complexes are capable of penetrating the lipid membrane; a mode of action that is not available to the salts, unless biotransformation complexes the salts. These considerations do not eliminate transport through protein channels but could act in addition to such mode of action.

V(V)-dipic ([VO_2dipic]$^-$) and Model Systems

A water in oil microemulsion comprised of the anionic synthetic surfactant, AOT, an organic solvent, and water has been used to examine the ability of V(V)-dipic to penetrate the anionic lipid interface (119). The structure of an AOT reverse micelle is found in Figure 4a. These systems were prepared from a solution of AOT in D_{12}-cyclohexane and aqueous V(V)-dipic dissolved in D_2O. 1D and 2D ^1H-^1H NOESY experiments were conducted to examine if interaction of AOT and V(V)-dipic was

occurring (119), where the results of the 2D ^{1}H-^{1}H NOESY show diagonal cross peaks and this indicates that the protons on the V(V)-dipic are near the protons in the methylene and methyl groups at the end of the AOT side chains, thus demonstrating that the drug penetrated the lipid interface even at this high concentration of complex (119). Since V(V)-dipic is an anionic vanadium complex, the location of this complex might have been expected to be in the water phase; however, the NOESY experiment indicates that the average complex location is interacting with the AOT sidechains that are presumed to be deep in the hydrophobic lipid interface.

Reverse micelles formed using the cationic surfactant, CTAB, combined with an alcohol (1-pentanol), an organic solvent (cyclohexane), and aqueous V(V)-dipic were also investigated (117 640). This quaternary system contains a positively charged head group which is likely to attract the negatively charged V(V)-dipic. Results from this study show that V(V)-dipic interacts presumably through Columbic forces with the cationic surfactant and is located at the aqueous interface. Studies using micelles were also carried out with the anionic ligand, dipic (E. Gaidamauskas, et al., in press). The V(V)-dipic complex was also found to associate with the micelle even though there was no confinement of the complex. This result suggests that the ligand and presumably the complex have an affinity for the interface as was reported for the reverse micelle, but details have not yet been reported (E. Gaidamauskas, et al., in press).

Combined, these studies show that although V(V)-dipic has a negative charge, it is able to penetrate a negatively charged lipid interface and is placed in the hydrophobic tails of the RM system. Although one might anticipate that this polar complex would remain in the polar water pool, it is stabilized near the tail ends of the anionic surfactant.

BMOV in its oxidized form, $[VO_2(ma)_2]^-$ and Model Systems

Studies have also been conducted investigating the behavior of BMOV's oxidized form, $[VO_2(ma)_2]^-$ bis(maltolato)dioxovanadium(V)) in reverse micellar and micellar systems using ^1H NMR spectroscopy (118). Aureliano and colleagues showed that changes in the spectroscopic signature of $[VO_2(ma)_2]^-$ are located at the polar end of the anionic surfactant, AOT (118). Therefore, any penetration of the $[VO_2(ma)_2]^-$ is limited to the polar head group of the lipid interface. Likewise, ^1H NMR has been used to investigate $[VO_2(ma)_2]^-$ and its interaction with CTAB micelles. This thesis investigates the penetration of $[VO_2(ma)_2]^-$ in CTAB reverse micelles analyzed via ^{51}V-NMR spectroscopy where signals where significantly broadened when compared to aqueous stock solution of $[VO_2(ma)_2]^-$ (further described in Chapter II). These results were interpreted as the $[VO_2(ma)_2]^-$ being associated with the interface but not deeply embedded in the lipid interface as described in detail in Chapter II. Studies with both the model system and the membrane Ca-ATPase preparation show that the $[VO_2(ma)_2]^-$ is associated with the membrane system, confirming the possibility that such interaction may take place *in vivo* and potentially affect the action of these compounds (118). See Figure 4b for CTAB micelle structure.

CONCLUDING REMARKS

This review provides a summary of the current literature discussing the effects vanadium compounds and salts on the structural components of the cell, specifically the organization of the cytoskeleton and plasma membrane. These articles demonstrate the diverse effects that vanadium compounds have on cellular function which can, in turn, affect ligand-mediated signaling and impact the activity of cellular enzymes. They also

suggest that it is important to investigate not only the chemistry and potential hydrolysis of various compounds *in vitro*, but to also investigate such compound function in various animal models and in model membrane systems.

To investigate interaction of vanadium compounds and salts with membrane interfaces (as discussed in Chapter I), NMR spectroscopy methods and two simple membrane model systems have been used together with an anti-diabetic compound in its oxidized form, $[VO_2(ma)_2]^-$ (discussed in Chapter II). We hypothesized that because this compound is negatively charged and, if placed in a positively charged model system, will interact with the model lipid. Our results in Chapter II of this thesis will help enhance our understanding of the mode of action of $[VO_2(ma)_2]^-$ in such systems.

Table 1: Vanadium compounds shown to down regulate gene expression of cytoskeletal components. Gene expression in *in vivo* diabetic animal models using various gene methods and animal models.

Gene Symbol	Gene Name	Compound	Animal Model	Method	Reference
Actn2	actinin alpha 2	$VO(alx)_2$[a]	ddY mice	Microarray	(55)
Actr3	actin-related protein 3 homolog	$VO(alx)_2$	ddY mice	Microarray	(55)
Flnc	filamin c, gamma	$VO(alx)_2$	ddY mice	Microarray	(55)
Myh3	myosin heavy chain	$VOSO_4$[b]	Wistar rats	Microarray; RT-PCR	(54)
Syne1	synaptic nuclear envelope 1	$VO(alx)_2$	ddY mice	Microarray	(55)
Tpm5	tropomyosin 5	$VOSO_4$	Wistar rats	Microarray	(54)
Tuba1c	tubulin, alpha 1C (tubulin, alpha 6)	$VO(alx)_2$	ddY mice	Microarray	(55)

[a] bis(allixinato)oxovanadium(IV); [b] vanadyl sulfate

Table 2: Vanadium compounds shown to down regulate gene expression of membrane proteins involved in carbohydrate metabolism/transport. Gene expression in *in vivo* diabetic animal models using various gene methods and animal models.

Gene Symbol	Gene Name	Compound	Animal Model	Method	Reference
Carbohydrate transport/metabolism					
Cebpa	CCAAT/Enhancer-binding protein (C/EBP), alpha	Na_3VO_4 [a]	SD [d] rats	NB[e]	(56)
Fbp2	Fructose bisphosphatase 2	$VO(alx)_2$	ddY mice	Microarray	(55)
--	Glucose-6-Phosphatase	BMOV [b]	Wistar rats	RT-PCR	(37)
Lyz	Type 1 and II of lysozyme C	$VOSO_4$	Wistar rats	Microarray	(54)
Ogt	O-linked N acetylglucosamine transferase	$VO(alx)_2$	ddY mice	Microarray	(55)
PEPCK	Phosphoenolpyruvate carboxykinase	BMOV; $NaVO_3$ [c]; $NaVO_3$	Wistar rats SD rats; Wistar rats	RT-PCR; NB	(37, 56, 59)
Phka1	Phosphorylase kinase alpha 1	$VO(alx)_2$	ddY mice	Microarray	(55)
Siat9	Ganglioside GM3 synthase	$VOSO_4$	Wistar rats	Microarray	(54)
GLUT2 transporter					
GLUT2	Glucose 2 transporter	Na_3VO_4	SD rats; Wistar rats	NB	(59)

[a] sodium orthovanadate; [b] bis(maltolato)oxovanadium(IV); [c] sodium metavanadate; [d] Sprague-Dawley; [e] Northern Blot

Table 3: Vanadium compounds shown to down regulate gene expression of proteins for lipid transport/metabolism. Gene expression in *in vivo* diabetic animal models using various gene methods and animal models.

Gene Symbol	Gene Name	Compound	Animal Model	Method	Reference
Lipid transport/metabolism					
Acaca	Acetyl-CoA carboxylase [a]	$NaVO_3$	Wistar/CPB rats	NB	(57)
Acsl3	Acyl-CoA synthetase long-chain family member 3	$VO(alx)_2$	ddY mice	Microarray	(55)
Aqp7	Aquaporin 7	$VOSO_4$	Wistar rats	Microarray	(54)
Apoe	Apolipoprotein E	$VOSO_4$	Wistar rats	Microarray	(54)
Cpt1a	Carnitine palmitoyltransferase 1	$VOSO_4$	Wistar rats	Microarray; RT-PCR	(54)
Decr1	Mitochondrial 2,4-Dienoyl-CoA reductase	$VOSO_4$	Wistar rats	Microarray; RT-PCR	(54)
Fabp3	Fatty acid binding protein 3	$VO(alx)_2$	ddY mice	Microarray	(55)
Fabp4	Fatty acid binding protein 4	$VOSO_4$	Wistar rats	Microarray	(54)
Fasn	Fatty acid synthase[b]	$NaVO_3$	Wistar/CPB[c] rats	NB	(57)
Hmgcs2	Mitochondrial 3-Hydroxy-3-methylglutaryl-CoA synthase	$VOSO_4$	Wistar rats	Microarray/RT-PCR	(54)
Hmgcs2	Mitochondrial 3-Hydroxy-3-methylglutaryl-CoA synthase	Na_3VO_4	SD rats	Northern blot	(56)
Lipe	Lipase (testicular isoform)	$VOSO_4$	Wistar rats	Microarray	(54)
Ppap2b	Phosphatidic acid phosphatase type 2B	$VO(alx)_2$	ddY mice	Microarray	(55)
Slc27a1	Fatty acid transport protein	$VOSO_4$	Wistar rats	Microarray	(54)

[a] Acaca was restored in rat liver cells, not in white adipose tissue; [b] Fasn was restored in rat liver cells and not white adipose tissues; [c]cardiopulmonary bypass rat model.

Table 4: Vanadium compounds shown to down regulate gene expression of proteins involved with insulin signaling. Gene expression in *in vivo* diabetic animal models using various gene methods and animal models.

Gene Symbol	Gene Name	Compound	Animal Model	Method	Reference
Irs1	Insulin receptor substrate 1	$NaVO_3$	Wistar rats	Microarray	(58)
Irs2	Insulin receptor substrate 2	$NaVO_3$	Wistar rats	Microarray	(58)
Dok1	Docking protein 1	$NaVO_3$	Wistar rats	Microarray; RT-PCR	(58)
Grb2	Growth factor receptor-bound protein 2	$NaVO_3$	Wistar rats	Microarray	(58)
Ptpn11	Protein tyrosine phosphatase non-receptor type 11	$NaVO_3$	Wistar rats	Microarray; RT-PCR	(58)
Ppp1ca	Protein phosphatase 1, catalytic subunit, alpha	$NaVO_3$	Wistar rats	Microarray; RT-PCR	(58)

Table 5: Vanadium compounds shown to up regulate gene expression of membrane proteins involved in carbohydrate and lipid transport/metabolism. Gene expression in *in vivo* diabetic animal models using various gene methods and animal models.

Gene Symbol	Gene Name	Compound	Animal Model	Method	Reference
Carbohydrate transport/metabolism					
Ckmt2	Mitochondrial creatine kinase	$VOSO_4$	Wistar rats	Microarray; RT-PCR	(54)
GK mRNA	Glucokinase	$NaVO_3$	SD rats; Wistar rats	NB	(56)
L-PK	L-type pyruvate kinase	$NaVO_3$	SD rats; Wistar rats	NB	(56, 59)
TAT	Gluconeogenic gene	$NaVO_3$	SD rats	NB	(56)
Lipid transport/metabolism					
Fasn	Fatty acid synthase	$VO(alx)_2$	ddY mice	Microarray	(55)
Scd1	Stearoyl-coenzyme A desaturase 1	$VO(alx)_2$	ddY mice	Microarray	(55)

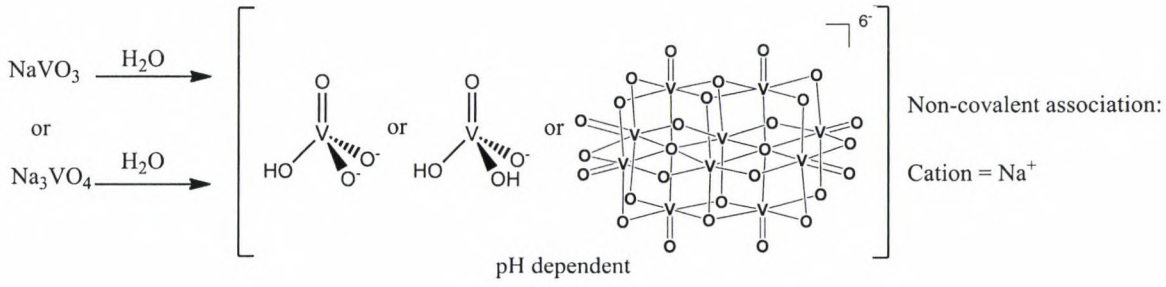

(a)

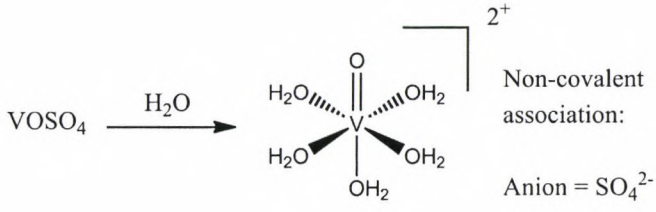

(b)

Figure 1: Vanadium salt formation in either a +4 or +5 oxidation state. (a) pH dependence on some forms of vanadium salts using the sodium cation where sodium metavanadate or orthovanadate ($NaVO_3$ or Na_3VO_4, respectively) are added to an aqueous solution. Additional oligomers are pH dependent and are described in (25). A few of the salts that form are vanadate(V) in its protonated and deprotonated form as well as decavanadate. (b) vanadyl(IV) formation by adding vanadyl sulfate to an aqueous solution. Structures from this figure were inspired by (6, 22, 23).

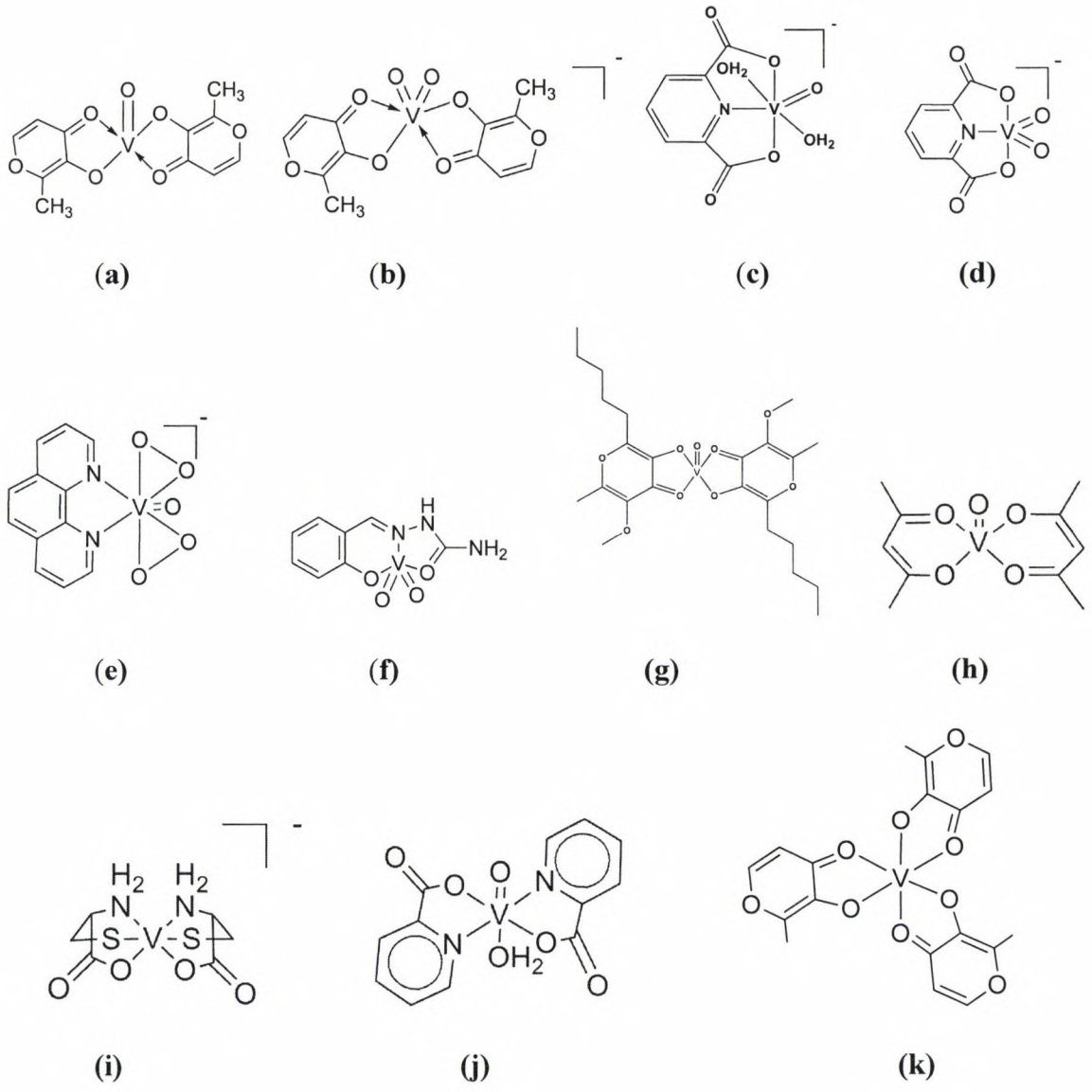

Figure 2: Structures of vanadium IV and V complexes. The abbreviation, name, and chemical formula of each structure discussed in this review are shown. (a) BMOV, bis(maltolato)oxovanadium(IV), $[C_{12}H_{10}O_7V]$; (b) $BMOV_{(ox)}$, bis(maltolato)-oxovanadium(V), $[C_{12}H_{10}O_8V]^-$; (c) V4dipic, pyridine-2,6-dicarboxylato-oxovanadium(IV), $[C_7H_7NO_7V]^-$; (d) V5dipic, pyridine-dicarboxylato-dioxovanadium(V), $[C_7H_3NO_6V]^-$; (e) V5phen; oxodiperoxo(1,10-phenanthrolin) vanadate; $[C_{12}H_8N_2O_5V]^-$; (f) V5-salsem, VO_2(salicylaldehyde semicarbazone), $[C_8H_8N_3O_4V]$ (122); (g) $VO(alx)_2$, bis(allixinato) oxovanadium(IV), $[C_{24}H_{34}O_9V]$; (h) $V(acac)_2$; bis(acac)oxovanadium(IV); $[C_{10}H_{14}O_5V]$; (i) V(III)-L-cysteine, $[C_6H_{10}N_2O_4S_2V]$; (j) $VO(pa)_2$; bis(picolinato)oxovanadium(IV), $[C_{12}H_{10}N_2O_6V]$ (38); (k) $V(ma)_3$; tris(maltolato)vanadium(III); $[C_{18}H_{15}O_9V]$.

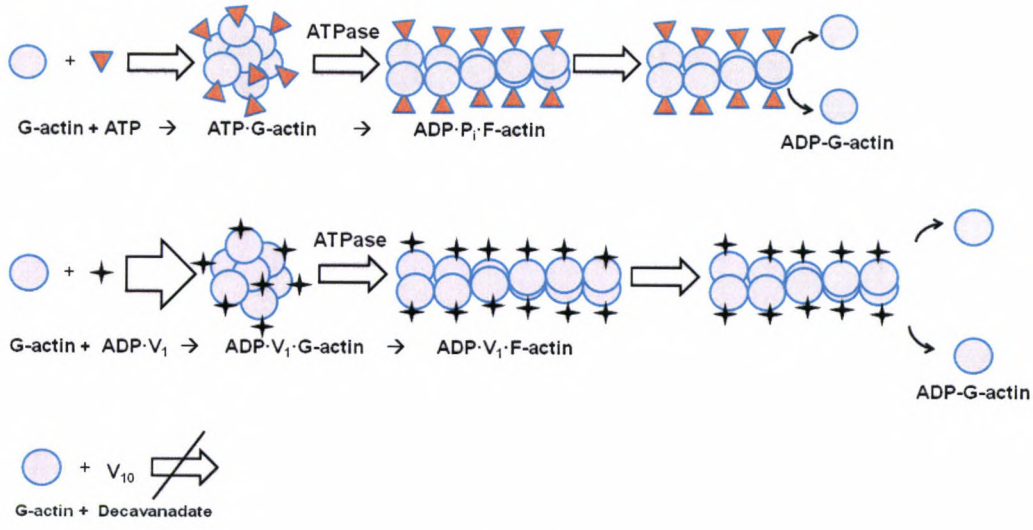

Figure 3: Vanadium's effects on actin polymerization process. This model demonstrates actin polymerization that has been represented in a number of science textbooks, indicating that this model is well accepted in the scientific community (123). The two literature models represent simplified diagrams that illustrate vanadium's interaction and effects with regulating actin polymerization. The illustrations above were generated from results and conclusions provided by (21, 61-64).

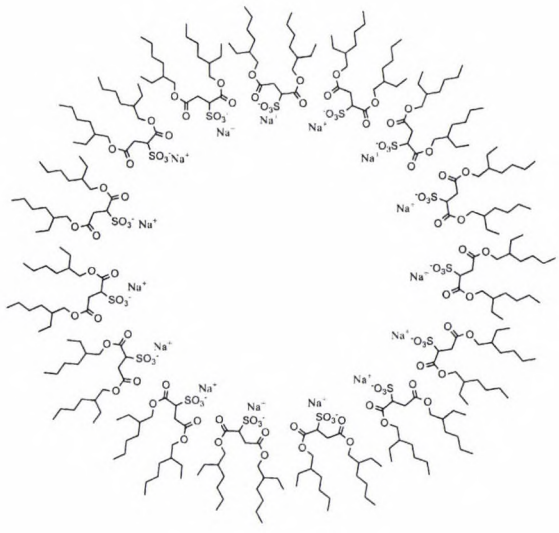

Figure 4: Structure of an aerosol-OT (AOT) reverse micelle system. AOT reverse micelles are composed of a surfactant, a non-polar solvent and an aqueous solvent typically containing the drug of interest.

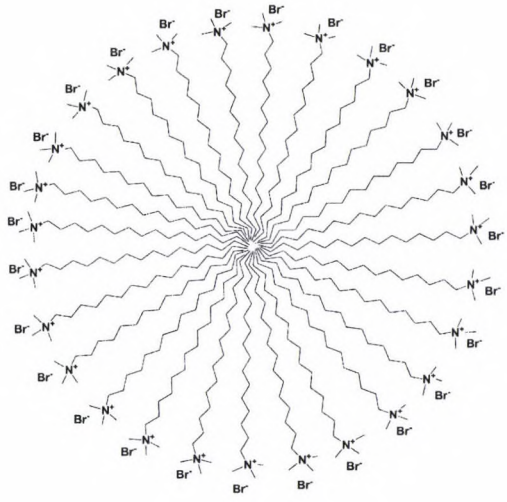

Figure 5: Structure of CTAB micelles. CTAB micelles are composed of a surfactant and an aqueous solvent usually containing the drug of interest. These micelle structures are composed of only two components, a surfactant and an aqueous solvent typically containing the compound of interest.

CHAPTER II[2]

ANTI-DIABETIC DRUG METABOLITES INTERACTING WITH MODEL MEMBRANE SYSTEMS: OXIDIZED BMOV IN CTAB MICELLES AND REVERSE MICELLES

INTRODUCTION

Understanding the interactions of drugs and their derivatives with plasma membranes is critical in evaluating the effectiveness of drug activity. We were interested in studying interactions of an oxidized metabolite of the anti-diabetic vanadium containing drug, bis(maltolato)oxovanadium(IV), abbreviated BMOV (Figure 6a), with membranes using a simple model membrane system (Figure 6a) (124). This study is motivated by recent reports suggesting that, in addition to the known inhibition of tyrosine phosphatases (39, 125-127), lipid interactions may impact the action of this class of anti-diabetic agent (12, 128).

---

[2] This chapter is adapted from a manuscript in preparation to be submitted to the *Journal of Biological Inorganic Chemistry*. Samantha K. Schoeberl, Debbie C. Crans, Bharat B. Baruah, Ernestas R. Gaidamauskas, Deborah A. Roess (2010). "Anti-diabetic drug metabolites interacting with model membrane systems: oxidized BMOV in CTAB micelles and reverse micelles".

The oxidized form of BMOV, abbreviated $[VO_2(ma)_2]^-$, (Figure 6b) is a vanadium(V) compound which readily forms upon administration of BMOV to rats in their drinking water (129). The structure of BMOV involves redox and hydrolytic processes and the effects of BMOV and metabolites have been considered independently in both *in vivo* and *in vitro* studies (130). The focus of this work was to investigate how the oxidized vanadium compound, $[VO_2(ma)_2]^-$ and the resulting hydrolysis products of vanadate and its oligomers as well as its ligand, maltol (Figure 6c) interact with membrane interfaces.

Cellular membranes are complex structures because of their heterogeneous composition of proteins and a diverse mixture of lipids. As an alternative to studying interactions of pharmacologic agents with poorly defined plasma membranes, model systems can be used. There are, however, both advantages and limitations to these model systems. Vesicle systems offer the advantage of maintaining the parent lipid bilayer structure and permit the study of a semi-stable system (131). Monolayer systems can be studied and include Langmuir monolayers (132), micelles (Gaidamauskas et al., in press) and reverse micelles (RMs); (21, 117).

Amphiphilic molecules that mimic lipid-lipid interactions can be used to model different aspects of the cell membrane (21, 23, 117, 119, 120, 133). Signal transduction typically occurs along the amphiphilic membrane layer and, therefore, structural similarities to model lipids including phosphatidylcholine has been considered (131). When using a positively charged surfactant, cetyltrimethylammonium bromide (CTAB); (Figure 7), for model studies, these interactions can be investigated and similar

interactions with complex membrane lipids inferred. This is particularly important when studying interactions between lipids and negatively-charged drugs.

Vanadium itself, in the +5 oxidation state is an effective probe for multinuclear NMR spectroscopy. Spectroscopic studies can investigate possible interactions of the drug with a CTAB micelle (Figure 8). The compound could potentially reside in the aqueous regions (a), the stern layer (b), or deep in the hydrophobic tail region (c) of the micelle. Alternatively in RMs, the drug could reside in the aqueous water pool (a), the interfacial region (b), or deep in the hydrophobic tail region (c). In Figure 9, the ^{1}H NMR spectra of the components for CTAB micelles and reverse micelles are shown. As illustrated in Figure 9, the chemical shift range for the complex is free for observation by ^{1}H NMR spectroscopy which allows for less complicated means for analyzing chemical shifts.

In this study, we were interested in examining whether one of the oxidized metabolites of the anti-diabetic drug BMOV penetrates membrane interfaces formed by CTAB. BMOV is a neutral drug and is generally believed to readily penetrate membranes. However, a recent study demonstrated that a negatively charged vanadium compound readily penetrates into the surfactant interface of model systems (119). The question addressed in this work will be how oxidized BMOV, $[VO_2(ma)_2]^-$, which is also negatively charged, interacts with two simple model systems created from surfactant with positively charged interfaces.

MATERIALS AND METHODS

Reagents

All chemical reagents were reagent grade and were used as received without further purification, unless indicated. $NaVO_3$, anhydrous (Aldrich, 99.9%); Maltol, $C_6H_6O_3$ (Aldrich, 99%); Cetyltrimethylammonium bromide (CTAB), $C_{19}H_{42}NBr$ (Sigma, 99%); filtered deuterium oxide, D_2O (Spectra Stable Isotopes); sodium deuteroxide, 30 weight % solution in D_2O (Aldrich, 99+ atom % D); deuterium chloride, 35 weight % solution in D_2O (Aldrich, 99 atom % in D); HPLC grade, submicron filtered cyclohexane, C_6H_{12} (Fisher Scientific); 1-pentanol (Aldrich).

CTAB was purified using anhydrous ethanol, the precipitated product was dried under vacuum overnight and stored in a dessicator containing anhydrous calcium sulfate solids (Drierite) until use (134). BMOV and $[VO_2(ma)_2]^-$ was synthesized as previously described (135).

Aqueous Stock Solution Preparation

A representative sample consisting of 200 mM $NaVO_3$ stock solution was prepared by adding 0.609 g to 15 mL D_2O in a 25 mL volumetric flask. The stock solution was then placed on a hot plate where constant mixing occurred until the solution was dissolved, which took approximately 1-2 hours to dissolve on low heat (approximately 35˚C. The solution was then removed from the hot plate to cool. After cooling, the pH of the solution was measured (pH ranged from 7.8-8) and was not adjusted. Additional D_2O was added to bring the volume to 25 mL. The solution was

then placed into a glass vial capped with a tephlon cap and with para film for storage at room temperature.

$[VO_2(ma)_2]^-$ was prepared from a 200 mM $NaVO_3$ aqueous stock solution where a representative sample solution consisted of 100 mM $NaVO_3$ and 200 mM maltol in a D_2O solution as described previously (135).

A representative 200 mM maltol stock solution was prepared by adding 0.126 g of maltol to a 5 mL volumetric flask with 3 mL of D_2O. The solution was placed on a hot plate with a stir bar on low heat (approximately 35˚C) until the maltol dissolved. The solution was then removed from the hot plate to cool. After cooling, the pH of the solution was recorded and adjusted if needed. D_2O was then added to a final volume of 5 mL. An important observation of maltol/D_2O solution is that if aqueous maltol solution experiences a dramatic temperature change, the maltol will immediately precipitate and the solution will change from colorless to a white, non-transparent solution.

$[VO_2(ma)_2]^-$ stock solution was prepared by adding 2.5 mL of 200 mM $NaVO_3$ stock solution to solid 0.126 g or 200 mM of solid maltol in a 5 mL volumetric flask. The solution was then placed on low heat (approximately 35˚C) on a stir plate with a stir bar until dissolved. Once dissolved, the solution was removed from the heat until it cooled. The addition of D_2O was then added to a final volume of 5 mL and pH adjusted as needed. It is important to note that because of maltol's hydrophobicity, it does not dissolve into D_2O; however, upon the addition of $NaVO_3$, maltol quickly dissolves and a slight-yellow appearance is immediately observed. The yellow appearance is distinctly different from the intense yellow color observed from decavanadate in aqueous solution.

Micelle Sample Preparation

CTAB micelle solutions were prepared by dissolving solid CTAB (Sigma, 99% purity) and $[VO_2(ma)_2]^-$ or maltol in deuterium oxide (D_2O). Samples were then incubated at 35°C until a transparent solution was observed and were held at 35°C in a warm water bath until they were analyzed via ^1H NMR. Once in the NMR, the samples were equilibrated for approximately 10 minutes at 35°C before they were analyzed. An example of sample concentrations is 50 mM of 99.9% purity CTAB dissolved in D_2O; 2 mM of aqueous $[VO_2(ma)_2]^-$ was then added to CTAB and D_2O and then placed in 35°C incubator until the sample was transparent and the sample remained at this temperature until analysis via NMR.

Reverse Micelle Sample Preparation

A representative 1 mL sample of a RM ($w_o = 4$) preparation is described. A 5:1 ratio of 1-pentanol:CTAB solution (136, 137) was prepared by weighing out 0.1 M of CTAB in a 3 mL tephlon capped glass vial. 1-pentanol was added with a glass syringe to 0.1 M of CTAB. Next, 938 µL of cyclohexane was added to the CTAB and 1-pentanol solution. At this point, the solution within the 3 mL glass vial displays a cloudy-white appearance. A 7.23 µL volume of aqueous stock solutions (containing probe and D_2O) of 0.1 M $[VO_2(ma)_2]^-$ or 0.2 M maltol were then added and the solution and mixed until the solution was transparent.

Preparation of Samples at Various pH

A Thermo Scientific orion 2-star pH benchtop meter and a VWR symphony gel epoxi semi-micro pH electrode 14002-766 were used to measure pH values of various samples.

Sample Characterization

Dynamic Light Scattering

Dynamic light scattering (DLS) and conductivity measurements were used to characterize CTAB micelles. Samples being analyzed via DLS experimentation were prepared, as described above, and filtered through a 0.2 μM disposable sterile nylon syringe filter prior to placing samples in a DLS 12 μL cuvette with a 8.5 mm center height. Prior to placing samples in the Dyna-Pro Titan DLS instrument, appropriate parameters (temperature, acquisition time, and laser power) were adjusted for appropriate CTAB micelle characterization. Representative CTAB micelle samples include a range from 50-250 mM of CTAB micelles in DI H_2O without $[VO_2(ma)_2]^-$.

Conductivity with CTAB Micelles

Conductivity samples were ran above the critical micelle concentration (*cmc*) for CTAB micelle formation of 1 mM concentration of CTAB. Conductivity samples were also ran above and below the Krafft Temperature (T_k) of CTAB, which is 23 ± 3°C (138). CTAB micelle samples were made with and without the addition of 2 mM $[VO_2(ma)_2]^-$ and instead of using D_2O as mentioned previously, samples were prepared with DI water.

Samples were made by following the micelle sample preparation method described above with varying concentrations of CTAB (8-40 mM).

NMR Spectroscopy Techniques

^{1}H NMR Spectroscopy of CTAB Micelles

Varian Inova 400 dual full-band (^{1}H to ^{103}Rh) NMR spectroscopy instrument was utilized to obtain ^{1}H NMR spectroscopy measurements of CTAB micelle and RM samples. Micelle and RM samples were prepared by following the stock solution preparations shown previously. Similarly, aqueous stock solutions consisting of the probe of interest in D_2O were prepared using similar methods as described above. The pH of the stock solution was adjusted as needed using the methods above. NMR instrumentation was first referenced using a DSS/D_2O mixture where the DSS peak was set to 0.000 ppm prior to running any NMR samples. Aqueous samples were referenced using the DSS/D_2O external referencing standard before aqueous samples were ran on the NMR. The micelle samples were referenced using either an external capillary NMR tube containing deuterated benzene (d-C_6D_6)/TMS mixture or using DSS/D_2O referencing standard. The d-C_6D_6 peak position was referenced to 7.157 ppm and the DSS peak position was referenced to 0.000 ppm.

CTAB micelle samples that were temperature sensitive were analyzed via the Varian Inova 300 dual full-band (^{1}H to ^{109}Ag) NMR spectroscopy instrumentation using the variable temperature feature set at 35°C. Samples were allowed to equilibrate in the instrument at that temperature for approximately 10 minutes prior to analysis.

^{51}V NMR Spectroscopy of Reverse Micelle Samples

Varian Inova 300 using ^{51}V NMR probe was used for CTAB RM samples containing $[VO_2(ma)_2]^-$ comparing $[VO_2(ma)_2]^-$ in D_2O with various w_o sizes. A $VOCl_3$ referencing standard was used prior to sample analysis.

2D-NOESY NMR Spectroscopy of Reverse Micelle Samples

Varian Inova 500 was used for CTAB RM samples containing 400 mM maltol in a w_o=20 RM. RM sample and aqueous samples was prepared using procedure described above.

RESULTS AND DISCUSSION

^1H NMR Results of $[VO_2(ma)_2]^-$ in Aqueous Solution

BMOV hydrolyzes into vanadium(IV) and maltol and reduces to $[VO_2(ma)_2]^-$ in aqueous solutions (135, 139). Although a detailed speciation study has been reported for $[VO_2(ma)_2]^-$, these studies were conducted using ^{51}V NMR spectroscopy. Little, if any, information is available using ^1H NMR studies in this system. Since we are focusing on studies with $[VO_2(ma)_2]^-$, we recorded the ^1H NMR spectra of $[VO_2(ma)_2]^-$ as a function of pH, and the data is shown in Figure 10. These data show that the complex hydrolyzes at pH value greater than 7. The observed pattern of complex hydrolysis as a function of pH is in accord Pettersson's group (139).

Interaction of $[VO_2(ma)_2]^-$ with CTAB micelles

We used ^1H NMR spectroscopy to probe the location of the $[VO_2(ma)_2]^-$ by exploring the effects on chemical shifts in different environments. If $[VO_2(ma)_2]^-$ complex penetrated into the CTAB micelle, then the protons located on the non-polar end of the CTAB molecule would have a larger change in chemical shift than protons on the polar head region of CTAB. This was further investigated by looking at the chemical shifts of CTAB above and below the critical micelle concentration (*cmc*) at which CTAB micelles form in solution. We used maltol ligand and $[VO_2(ma)_2]^-$ complex to examine whether such interactions were occurring; results support that interaction is occurring for both compounds.

Given the pH dependence of $[VO_2(ma)_2]^-$ speciation, we investigated the interaction of this complex with CTAB micelles at pH 7, 8, and 9. CTAB forms micelles in aqueous solution above 35°C and above the *cmc* concentration ranging from 0.86 mM (140) to 0.96 mM (141), where below this value, CTAB exists in its monomeric form that is distributed in aqueous solution. One series of ^1H NMR spectra of 2 mM $[VO_2(ma)_2]^-$, and 50 mM CTAB are shown in Figure 11 at pH values of 7.4, 8.2, and 9.1. The ^1H NMR spectra shows how the proton chemical shifts of $[VO_2(ma)_2]^-$ change as a function of pH and, when compared to the results of proton chemical shifts in an aqueous solution, information on the changes in the environment of the complex is obtained. The protons that correspond to the appropriate peaks for $[VO_2(ma)_2]^-$ are labeled, ^{C}Ha and ^{C}Hb, and show different shifts which provide support on the details of the location of $[VO_2(ma)_2]^-$. No change was observed at the different pH values for the $[VO_2(ma)_2]^-$; however, placing the complex in the presence of CTAB did result in an upfield chemical shift. Since this

change is not significantly observed for the $[VO_2(ma)_2]^-$ below the *cmc*, we conclude that the observed effect is due to $[VO_2(ma)_2]^-$ interaction with the interface of the micelle.

To confirm the studies shown in Figure 11 in which $[VO_2(ma)_2]^-$ is shifting in the presence of CTAB, we investigated the effects that this probe had on CTAB chemical shifts as the concentration of CTAB was varied. If the probe penetrates the CTAB interface, one would expect some changes in the CTAB chemical shifts. In Figure 7, we show the labeling of CTAB. As shown in Figure 12a we see that the chemicals shift for the alpha and $^+N(CH_3)_3$ protons are the parts of the CTAB molecule with greatest changes (Figure 12a). However, since some of these effects can be due to CTAB micelle formation, we compared these chemical shifts to that of CTAB micelle formation in the absence of probe. This is shown in Figure 12b. Comparing the shifts in Figure 12a and 12b we see that the major change is only with the alpha proton. This information suggests that the $[VO_2(ma)_2]^-$ complex is only interacting with this proton.

In addition to upfield chemical shifting as $[VO_2(ma)_2]^-$ was placed in a CTAB micelle that was illustrated in Figure 11, we observed hydrolysis of $[VO_2(ma)_2]^-$ as the pH was varied. Therefore, we integrated the CH_3 group of both complex and maltol and were able to successfully determine the ratio of complex hydrolysis comparing aqueous with micelles at pH levels below, near and above the pK_a of maltol of 8.27 (135, 139). Results showed that in aqueous solution, $[VO_2(ma)_2]^-$ does not hydrolyze as a change of pH indicating that the complex is stable at different pH values in aqueous solution. However, when $[VO_2(ma)_2]^-$ is placed in a CTAB micelle solution, the pH becomes more favorable for deprotonation of maltol where complex hydrolysis is occurring and maltol peaks are presented in the ^1H NMR spectra shown in Figure 11. In Table 6, we show the

ratio of complex hydrolysis as a function of pH in comparing aqueous samples with micelles. To determine the ratio of complex hydrolysis, *equation 1* was used:

$$\frac{[\text{complex}]}{[\text{complex}] + [\text{ligand}]} \qquad \textit{equation 1}$$

At a pH of around 9 for micelles, there is only 25% complex present in solution while 91% complex is present in aqueous solution. For micelle samples, as the pH decreases, there is more complex present in solution than maltol. Therefore, pH has an effect on the stability of the $[VO_2(ma)_2]^-$ in the presence of CTAB and no effect when in an aqueous solution consisting only of D_2O.

Characterization of Micelles via Conductivity Studies

Conductance of micelle solutions was used to characterize the *cmc* for the particular system being investigated. Changes in conductivity of the sample as the concentration of the surfactant was varied allowed one to determine the *cmc* of the surfactant. Studies have been conducted that examine the *cmc* of CTAB and they have seen a drastic change in conductance at approximately 1 mM of CTAB (140, 141). In addition to determining the *cmc* of the surfactant, conductivity has also been used to determine the Krafft temperature (T_k) of various surfactants, specifically CTAB (138) where the T_k has been identified at 26°C (142). Based on current literature values and trends of drastic changes in conductance at the *cmc* for CTAB, we hypothesized that if we are properly making CTAB micelles in solution, we will see similar trends above the *cmc* of CTAB and near the T_k of CTAB.

Conductivity characterization of micelles above *cmc* at temperatures above and below the T_K of 26°C (142) with and without 2 mM of $[VO_2(ma)_2]^-$ were performed. Since temperature and concentration are such key contributors of the conductivity of samples and are important factors in proper CTAB micelle formation, two different temperatures, 20°C and 30°C, were explored at different CTAB concentrations. The selected temperatures are above and below the T_K at which micelles begin to aggregate and form micelles. Figure 13 shows that as the concentration of CTAB increases the conductivity of the sample increases. Also, as the temperature is increased, conductivity increases slightly as well.

To investigate $[VO_2(ma)_2]^-$ effects on conductivity of the micelle samples, the conductance of samples containing probe and no probe was compared. Our results showed that when $[VO_2(ma)_2]^-$ was added to the system, the conductivity increased.

Based on ^1H NMR results from $[VO_2(ma)_2]^-$ in aqueous samples and CTAB micelles, we then investigated the probe's effect on chemical shifts of CTAB. Based on slight changes in the alpha group on CTAB when $[VO_2(ma)_2]^-$ was present, we were able to diagram two proposed models of $[VO_2(ma)_2]^-$ interaction with the micelle interface and its penetration into the polar head region of the CTAB micelle, also called the stern layer (133) (Figures 14a and b).

Interaction of the Ligand, Maltol, with CTAB Micelles

Based on the previous results, we hypothesized that, if maltol ligand deeply penetrates into the micelle, the protons located on the nonpolar end of the CTAB molecule should have a larger change in chemical shift than the protons on the polar head

region of CTAB. This hypothesis can be further investigated by looking at the chemical shifts of CTAB above and below the *cmc*.

Since $[VO_2(ma)_2]^-$ hydrolyzes to form vanadate and maltol, we examined the effects of CTAB on maltol. However, at neutral pH, the complex is stable and only small amounts of maltol is observed, so additional spectra were recorded. Because effects due to exchange between complex and ligand had to be ruled out, and therefore spectra were also recorded of maltol at the higher pH values. Maltol is known to deprotonate as the pH increases and as compounds deprotonate, there is upfield chemical shift in ^{1}H NMR spectroscopy (143). In literature, proton chemical shifting of compounds when placed in micelle or RM systems have suggested that penetration of the probe occurs into the interfacial layer of the system (117, 118). Therefore, one question that can be asked is whether the upfield chemical shifting observed is due to penetration into the micellar interface or deprotonation of maltol. We first examined maltol's interaction with CTAB micelles using pH values above, near, and below the pK_a value for maltol which is at a value of 8.4 (139). It is important to examine maltol above its pK_a because the compound is deprotonated above this pH and any chemical shift that is observed in micelles will not be due to deprotonation, but rather penetration into the micelle interface.

As mentioned previously, $[VO_2(ma)_2]^-$ hydrolysis occurs; therefore, it is important to investigate the ligand, maltol, without vanadium in solution. One ^{1}H NMR series of 4 mM maltol in aqueous and CTAB micelles at a concentration of 50 mM CTAB is shown in Figure 15 at approximate pH values of 7, 8 and 9 (Figure 15). The ^{1}H NMR spectra shows that below maltol's pK_a, there are no significant chemical shifts identified in aqueous samples, but that upfield shifts are observed when maltol is placed into a

micelle. Above its pK_a, aqueous maltol shifts upfield which demonstrates deprotonation as shown in Figure 10. Further upfield chemical shifting is observed when maltol is negatively charged and placed into a CTAB micellar solution. Figure 16 shows two possibilities of maltol interaction with micelles based on the results described above.

Interaction of oxidized BMOV, $[VO_2(ma)_2]^-$, with CTAB/1-Pentanol/Cyclohexane/ D_2O Reverse Micelles

In addition to the studies of $[VO_2(ma)_2]^-$ with micelles, the interactions with CTAB/1-pentanol reverse micelles (RMs) was examined using ^1H NMR spectroscopy. The effects of different RM sizes on chemical shifts and the effects of pH was investigated to gauge the location of the complex. If $[VO_2(ma)_2]^-$ is penetrating into the RM interface, the protons located on the complex will have a change in chemical shift as the environment changes from aqueous to RM. However, if the interaction is strictly with the interface, changes should reflect how deeply penetration is as the size of the RM is modified.

Because of the changes in speciation with pH of $[VO_2(ma)_2]^-$, the interactions of $[VO_2(ma)_2]^-$ with a series of different sized RMs was explored both at neutral and basic pH. The $[VO_2(ma)_2]^-$ complex is most stable near neutral pH and hydrolyzes in samples outside the stability window. No changes were observed in the complex chemical shift at varying pH; however, the presence of a signal upfield to the $[VO_2(ma)_2]^-$ report on complex hydrolysis and the formation of protonated maltol (Figure 10).

In Figure 17, the ^1H NMR spectra are recorded of 100 mM stock solutions of $[VO_2(ma)_2]^-$ pH 7.0 in 200 mM CTAB with 1-pentanol in cyclohexane using a

water:surfactant ratio that defines that size of the RM, termed the w_o. The size of the RM can be determined by *equation 2*.

$$w_o=([H_2O]/[CTAB]) \qquad \textit{equation 2}$$

W_o values ranged from 6 to 20. In Figure 17 the entire spectrum window ranging from -0.05ppm to 9 ppm is shown (left). The signals assigned to $[VO_2(ma)_2]^-$ and free maltol are decreasing in intensity as the w_o size decreases and thus reflect the smaller size of aqueous water pool. As a result of this observed change in intensity, an insert is included focusing just on the Ha and Hb proton signals for the $[VO_2(ma)_2]^-$ complex and the product of hydrolysis, maltol (right) (Figure 17).

As w_o size decreases, $[VO_2(ma)_2]^-$ protons shift slightly upfield when comparing it to aqueous solution at a physiological pH of 7. The small chemical shift changes for the complex indicate that the protons on $[VO_2(ma)_2]^-$ are located in a polar environment similar to bulk water. These data suggest that if $[VO_2(ma)_2]^-$ interacts with the lipid interface, the interaction must be a weak interaction or is countered by potential interface interactions. It is also possible that the complex may be located in the water pool of the RM system, or that the environment at the lipid interface has similar polarity to that of water. Examples currently exist for several of these possibilities (23, 117-120). If the complex is located in the water pool and it is approaching the interface as the RM size decreases, a large change would be observed with decreasing w_o. However, our data supports that only a modest change in chemical shifting as the w_o size decreases is observed (Figure 17).

To further explore this system, the ^{51}V NMR spectra were recorded of solutions containing 100 mM $[VO_2(ma)_2]^-$ and 100 mM CTAB. As shown in Figure 18 and Table

8 the ^{51}V NMR spectra indicate that the signals for $[VO_2(ma)_2]^-$ show a slight downfield shift as the w_o decrease (Figure 18 and Table 8). These observations are in accord with the previous studies reported for $[VO_2(ma)_2]^-$ in AOT/isooctane (118). In addition, larger downfield shifting for ^{51}V NMR has been reported recently for $[VO_2dipic]^-$ in CTAB/*n*-pentanol/cyclohexane RMs (117) and for V_{10} in AOT/isooctane RM (23). No change in ^{51}V NMR chemical shift was observed with $[VO_2dipic]^-$ in AOT/isooctane RMs (119). The most significant change in the $[VO_2(ma)_2]^-$ signal upon placement in the RM is the increasing line width as the w_o decreases. This significant change in linewidth for ^{51}V NMR studies as the w_o decrease is generally associated with immobilization of a vanadium complex. In aqueous solution, vanadium complexes are able to rotate freely in solution and this is represented by the sharp ^{51}V NMR peak at -496 ppm. Similar observations of peak linewidth compared to that in aqueous solution might also be observed and the data would suggest that the complex is located in the aqueous pool and approaching the interface as the w_o decrease. This dramatic change in line width was previously observed for V_{10} in AOT/isooctane RMs (23, 120). The spectra shown in Figure 18 are in contrast to observation with $[VO_2dipic]^-$ in CTAB/1-pentanol/cyclohexane RMs, where no change was found as the w_o changed and the linewidth was above 1100 Hz for all the w_o samples investigated (117). Several other systems have been reported in which changes in the line widths were found as the w_o decreased, these include the V_{10} in AOT/isooctane RMs (23, 120) $[VO_2(ma)_2]^-$ in AOT/isooctane (118). In fact, these studies do suggest that complex is associated with the water pool, and that decreasing the w_o size will promote the complex to approach the interface due to the decrease in water pool size.

To compare chemical shifts of $[VO_2(ma)_2]^-$ at a pH of 9.7 with previous results at pH 7, a w_o series consisting of 100 mM $[VO_2(ma)_2]^-$, 200 mM CTAB, and 1-pentanol in cyclohexane as a function of pH were recorded through ^1H NMR techniques. Figure 19 shows the ^1H NMR spectra at pH 9.7 where the entire spectrum ranging from -0.05 to 9 ppm is shown on the left and a spectra to the right provide focus on the Ha and Hb protons for both, $[VO_2(ma)_2]^-$ and maltol (Figure 19).

Results show that as w_o size decreases, the protons in $[VO_2(ma)_2]^-$ shift very little when comparing them to aqueous solution at pH 7 (Figure 17). The small chemical shift changes indicates that the protons on $[VO_2(ma)_2]^-$ are located in a polar environment similar to bulk water. The small shifts at pH 9.7 support the observations made at pH 7, and are consistent with the recognition that no change in the complex is observed as the pH is changed from neutral to more basic. However, as shown for samples at pH 7, hydrolysis of $[VO_2(ma)_2]^-$ is also observed as the w_o size decreases and free maltol ligand is formed in these solutions; clearly shown by the decrease in peak intensity of $[VO_2(ma)_2]^-$ and the increase in maltol ligand intensity. To better interpret this data, studies were carried out only with the maltol ligand as described below.

Since the $[VO_2(ma)_2]^-$ protons (^{C}Ha) are not shifting as the w_o size decreases this indicates that the ^{C}Ha protons on the complex are remaining in the same environment as bulk water. This would be possible if the proton was near/in the waterpool or in the interface of the RM. The ^{C}Hb proton on the complex are shifting upfield as the w_o size decreases, which suggests that it is penetrating into the interface layer of the RM. The methyl group located on the complex is not shifting as the w_o size changes and has the same chemical shift as $[VO_2(ma)_2]^-$ in D_2O which suggests that the methyl group is

located in the aqueous water pool of the RM. This conclusion was supported by the ^{51}V NMR studies, that show that the line width of $[VO_2(ma)_2]^-$ increase as the water pool is smaller, and is consistent with the complex being associated with the changed environment in the water pool as illustrated in a schematic drawing in Figure 21.

Interaction of Maltol with CTAB/1-Pentanol/Cyclohexane Reverse Micelles

Our next task was to investigate the interaction of maltol and its behavior in CTAB/1-pentanol/cyclohexane RMs to confirm the interpretations made with the $[VO_2(ma)_2]^-$ complex, and the accompanying hydrolysis of complex in RMs. The pK_a for deprotonation of maltol at 8.7 (139) results in upfield chemical shift changes because the change in maltol protonation states. In Table 7, the Ha proton shifts 0.1 ppm, the Hb proton 0.2 ppm and the CH_3 proton 0.1 ppm as pH change from 7 to 9.7 in aqueous solution.

In Figure 20 the chemical shifts of each proton in maltol are compared to that in aqueous solution. Focusing on CH_3 on maltol first the upfield shifts are 0.05 ppm at all pH values examined. At pH 7.0, at all w_o sizes (4-20) there is a large upfield shift for the Hb proton when comparing it to aqueous stock solution. However, the Ha proton show no significant shifting upon placement in the CTAB/1-pentanol/cyclohexane RM. At pH 9.7, at large w_o sizes (16 and 20) there is no significant shift for the Hb proton when comparing it to aqueous stock solution at pH 9.7. However, when the w_o size is smaller (4-10), there is an upfield chemical shift from the aqueous stock solution as the w_o size decreases. However, the ^{L}Ha proton exhibit a downfield chemical shift upon placement in the CTAB/1-pentanol/cyclohexane RM, and this shift does not change with the w_o size of the RM. Combined, these data show that the chemical shifting of the maltol ligand in

the absence of vanadium complex is identical to that observed in the presence of complex.

In describing the orientation of maltol in the RM system, it is important to examine the shifting of each proton of maltol. At pH 7, below the pK_a, the ^{L}Hb on maltol has an upfield chemical shift whereas ^{L}Ha has no significant shift from aqueous. This suggests that ^{L}Ha is not interacting with the lipid interface and is located in the aqueous water pool. The methyl group is displaying an insignificant change in the chemical shift when comparing it to aqueous, which indicates that it is remaining in the aqueous water pool of the RM or a similarly polar environment as the ^{L}Ha proton. Since the ^{L}Hb proton does not approach the aqueous sample in regard to its chemical shift, this suggests that it is located in a different environment than the water pool. When comparing the chemical shifts of ^{L}Ha of maltol, it approaches the chemical shifts of the aqueous maltol/D_2O sample, which implies that it is located in a polar environment similar to aqueous solution.

There are two contributing factors that are associated with a chemical shifting of maltol, deprotonation or penetration into the RM system. These factors become more confusing when we discuss different levels of penetration in regard to upfield vs. downfield chemical shifting. When protons shift downfield, the proton is penetrating deep into the hydrophobic region of the RM. However, when the proton is located near the aqueous or head group of the RM, an upfield shift occurs. Deprotonation of compounds display upfield chemical shifting while the compound is deprotonating (143). When we examined whether maltol was capable of penetrating into the RM system, deprotonation and penetration were both potential contributing factors. Therefore, we

examined the pH above, near, and below the pK_a of maltol. When examining pH 9.7 at which maltol is deprotonated, any upfield chemical shifting cannot be explained as deprotonation, but rather penetration. At lower w_o sizes of 4-10, the $^{L}CH_3$ and ^{L}Hb on maltol display a further upfield chemical shift than the aqueous sample of completely deprotonated maltol (pH 9.7). ^{L}Ha displays very interesting results because at pH 9.7, there is a downfield chemical shift which would suggest that ^{L}Ha is penetrating into the lipid interface. There is no significant chemical shift of ^{L}Ha at pH 7, except at w_o 4. No significant chemical shift from aqueous would suggest that ^{L}Ha is remaining in the water pool of the RM. Figure 22 shows an example of how maltol is interacting with the RM based on our findings. In addition, Table 9 provides numerical data showing upfield chemical shifts of maltol as a function of w_o size.

DISCUSSION

Complex and Maltol in CTAB Micelles

Recent studies have shown that upfield chemical shifts of compounds of interest indicate that the compound resides deep in the cationic micelle system (near the hydrophobic tail region of CTAB). Our studies were conducted above and below the pK_a of 8.63 in micelles and aqueous solution. Because of an upfield shift in aqueous maltol as the pH increases above the pK_a, deprotonation of the ligand is occurring. In the literature, upfield chemical shifting represents deprotonation of the compound being investigated, such as maltol (143). When maltol is placed in CTAB micelles there is an upfield chemical shift of the protons consistent with penetration of the probe into the micelle. Therefore, the protons located on maltol show an upfield chemical shift; therefore the free ligand must be penetrating into the micelle and displays a similar

behavior to that of $[VO_2(ma)_2]^-$. Also as the ligand becomes deprotonated, there is a greater upfield chemical shift which implies that, as the ligand becomes more negatively charged, the electrical environment of the proton changes from more polar (aqueous solution) to more non-polar (interaction with model system). Since CTAB is positively charged, one would expect the molecules to be attracted to one another and this is evident through the upfield chemical shifts of the protons on the deprotonated maltol.

When looking at chemical shifts for ^1H NMR studies, penetration and deprotonation can be occurring in the samples. In order to determine if the shifting is due to deprotonation or location in the micelle, chemical shifts of CTAB must be further examined. CTAB does not show a significant shift from pH 7 to pH 9 when $[VO_2(ma)_2]^-$ and its hydrolyzed product, maltol, are placed in solution. This indicates that, even though maltol becomes more electronegative as the pH increases, there is no preference in regard to its location based on its charge. One would expect that the more negative a compound is, the more likely it would be attracted to the positively charge surfactant; likewise, more upfield shifting would indicate further penetration into the hydrophobic region of the CTAB micelle. While we see further upfield shifting, we can conclude that it is due to deprotonation and not to further penetration into the micelle.

The aqueous maltol solutions shift upfield when the pH is increased and it has been concluded in other literature that it is due to deprotonation of the probe. Although this may be the case, there is still an upfield shift when comparing aqueous solutions with micelle solutions, indicating penetration of ligand.

Maltol in CTAB Reverse Micelles

The protons on the maltol ligand shift differently depending on protonation state and thus support a slight readjustment of the probe location upon changes in charge. The small chemical shifts indicate that the Hb protons, upon deprotonation of maltol, are in a polar environment similar to bulk water whereas the Ha proton may be penetrating the hydrophobic interface region. This differs from observations with the neutral and protonated probe in which the Ha proton remains in the polar interface region and the Hb might be penetrating the lipid interface. The two proposed orientations are shown in Figure 23. Undoubtedly, the positively charge CTAB interface favors interactions with negatively charged counterions such as deprotonated maltol. Thus, it is not clear why the neutral maltol ligand simply does not deprotonate to form a similar arrangement. Many factors could be invoked such as the H-bonding to the OH group in the stern layer and the interactions between CTAB and maltol that we have seen for micelles is favorable.

Table 6: Ratio of 2 mM $[VO_2(ma)_2]^-$ hydrolysis in 50 mM CTAB micelles and aqueous solution as a function of pH. Ratios above 0.5 indicate that there is more complex present than free maltol ligand.

	pH 7	**pH 8**	**pH 9**
Micelle	0.66	0.63	0.25
Aqueous	0.91	0.91	0.91

Table 7: Maltol, $[VO_2(ma)_2]^-$, and CTAB chemical shifts as a function of pH.

		Probe Chemical Shifts				CTAB Chemical Shifts				
Probe	**pH**	**Ha**	**Hb**	**CH_3**	**[CTAB], mM**	**$^+N(CH_3)$**	**α-CH_2**	**β-CH_2**	**δ-CH_2-$(CH_2)_{11}$**	**ω-CH_3**
-	7.2	-	-	-	0.2	3.07	3.27	1.75	1.26	0.84
-	7.2	-	-	-	10	3.16	3.38	1.76	1.29	0.87
-	7.2	-	-	-	20	3.16	3.39	1.76	1.29	0.87
Maltol	7.4	6.43	7.89	2.26	50	3.13	3.38	1.72	1.24	0.82
Maltol	8.0	6.39	7.84	2.29	50	3.13	3.38	1.72	1.24	0.82
Maltol	9.3	6.32	7.69	2.26	50	3.13	3.37	1.71	1.24	0.82
Maltol	7.0	6.51[a]	7.99	2.37	0	-	-	-	-	-
Maltol	9.7	6.40	7.85	2.32	0	-	-	-	-	-
Maltol	10.3	6.40	7.83	2.31	0	-	-	-	-	-
Maltol	10.8	6.34	7.79	2.28	0	-	-	-	-	-
$[VO_2(ma)_2]^-$ *	6.9	6.45	7.95	2.35	50	3.13	3.39	1.72	1.24	0.82
$[VO_2(ma)_2]^-$ *	7.9	6.45	7.95	2.35	50	3.13	3.39	1.72	1.24	0.82
$[VO_2(ma)_2]^-$ *	9.0	6.45	7.96	2.35	50	3.13	3.38	1.72	1.24	0.81
$[VO_2(ma)_2]^-$ #	9.1	6.48	7.99	2.39	50	3.16	3.39	1.76	1.28	0.86
$[VO_2(ma)_2]^-$	7.0	6.51 [a]	8.06	2.42	0	-	-	-	-	-
$[VO_2(ma)_2]^-$	9.7	6.53	8.06	2.42	0	-	-	-	-	-
$[VO_2(ma)_2]^-$	10.3	6.53	8.05	2.42	0	-	-	-	-	-
$[VO_2(ma)_2]^-$	10.8	6.5	8.03	2.39	0	-	-	-	-	-

* These samples were ran using a DSS/D_2O referencing standard set at 0.000 ppm using Inova 400 NMR spectroscopy; # Micelle samples were ran using a TMS/d-benzene external referencing standard using Inova 300 NMR spectroscopy; [a] Proton chemical shifts of $[VO_2(ma)_2]^-$ and maltol are not easily distinguishable due to signal overlapping.

Table 8: ^{51}V NMR chemical shifts and linewidth values in RM systems.

w_o size	δ, ppm	Linewidth (Hz)	Probe	Surfactant	Cosurfactant	Reference
Stock	-496.90	486 ± 8	$[VO_2(ma)_2]^-$	-	-	This work
Stock	-495.6	420± 3	$[VO_2(ma)_2]^-$	-	-	(118)
20	-493.71	1075 ± 41	$[VO_2(ma)_2]^-$	CTAB	1-pentanol	This work
20	-495.2	630 ± 6	$[VO_2(ma)_2]^-$	AOT	-	(118)
20	-529.8	1160 ± 30	$[VO_2dipic]^-$	CTAB	Amyl alcohol	(117)
10	-496.07	- [a]	$[VO_2(ma)_2]^-$	CTAB	1-pentanol	

[a] linewidth values were not recorded at this w_o size.

Table 9: Chemical shift values of maltol protons as a function of w_o size. Samples were prepared at a pH value of 8.27.

	Maltol Chemical Shifts		
w_o size	**Ha**	**Hb**	**CH_3**
4	6.43	7.71	2.30
6	6.45	7.74	2.30
8	6.45	7.75	2.31
10	6.45	7.75	2.31
20	6.45	7.77	2.32
Stock	6.47	7.95	2.36

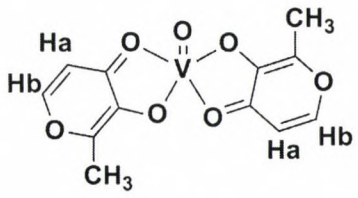

(a) BMOV

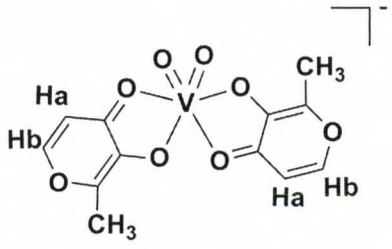

(b) Oxidized BMOV, abbreviated $[VO_2(ma)_2]^-$

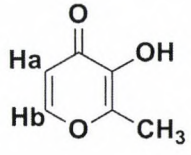

(c) Maltol

Figure 6: Structures of BMOV (a), oxidized BMOV abbreviated $[VO_2(ma)_2]^-$ (b) and maltol (c).

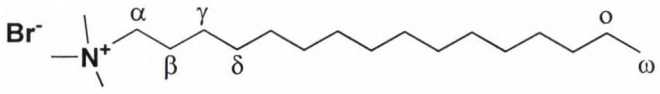

(a)

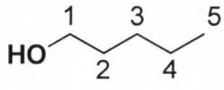

(b)

Figure 7: Structures of cetyltrimethylammonium bromide (a) and 1-pentanol (b).

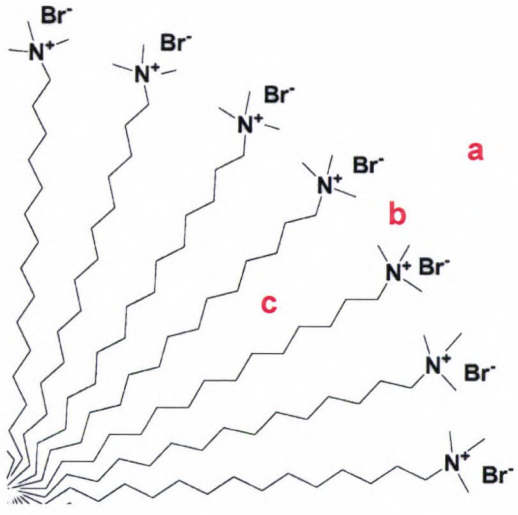

(a)

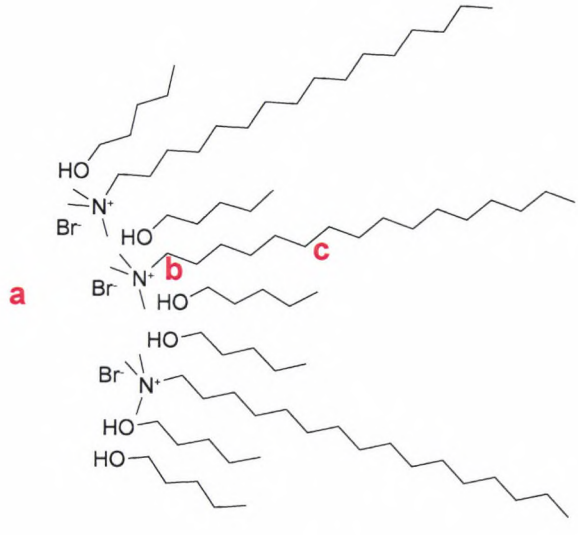

(b)

Figure 8: Diagram of possible drug location in CTAB micelles (a) and reverse micelles (b).

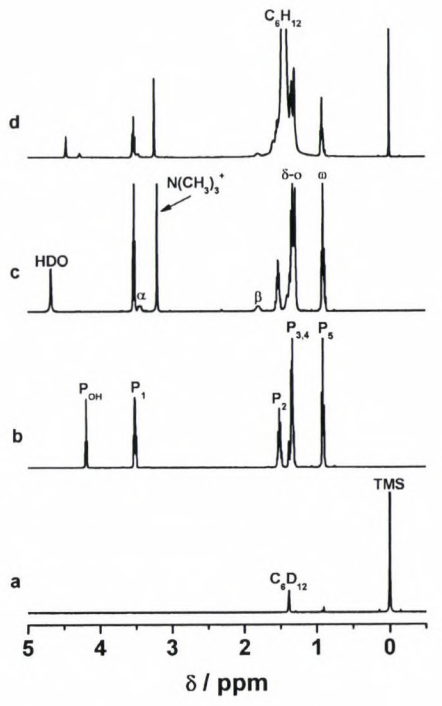

(a)

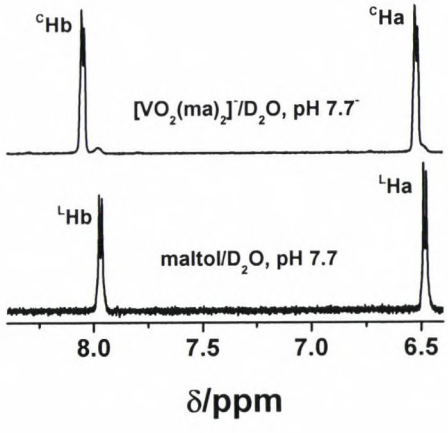

(b)

Figure 9: ^{1}H NMR spectra illustrating chemical shifts of various components used in this study. Peak assignments for various components are included. A: (a) d_{12}-cyclohexane (C_6D_{12}) and TMS; (b) 1-pentanol chemical shifts represented by P_x; (c) CTAB (represented by greek alphabet), 1-pentanol, D_2O, and C_6D_{12}; (d) CTAB, 1-pentanol, D_2O and C_6H_{12}. B: ^{C}Hb and ^{C}Ha represent protons located on $[VO_2(ma)_2]^-$ and ^{L}Ha and ^{L}Hb represent protons located on maltol.

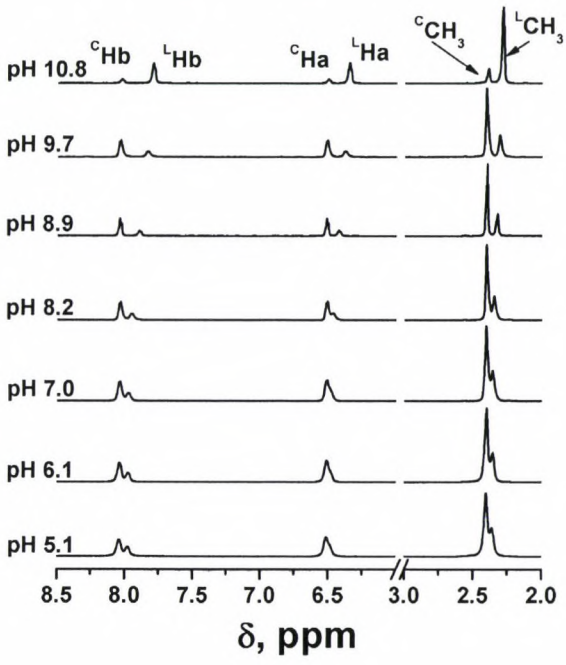

(a)

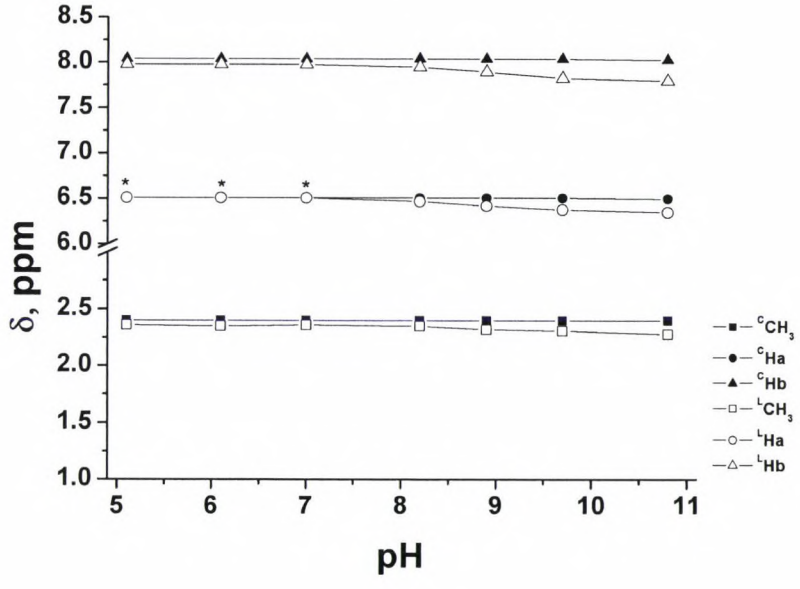

(b)

Figure 10: Aqueous samples containing $[VO_2(ma)_2]^-$ in D_2O as a function of pH. The HDO peak that appears around 4.8 ppm was removed from the spectra for simplistic purposes. Proper peak labeling is shown where ^{C} represents complex ($[VO_2(ma)_2]^-$) and ^{L} represents maltol ligand. (a) ^1H NMR spectra of complex and maltol chemical shifts as a function of pH. (b) * indicates that $[VO_2(ma)_2]^-$ and free maltol ligand peaks are overlapping and thus, not able to be distinctly identified separately.

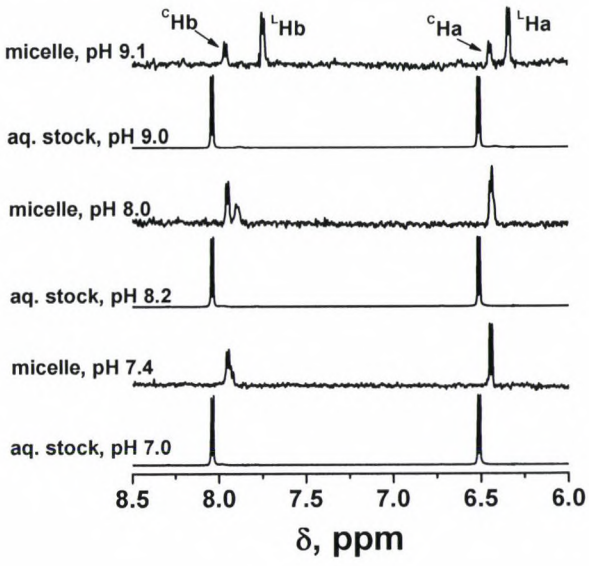

Figure 11: Chemical shifts of 2 mM $[VO_2(ma)_2]^-$ and maltol protons as a function of pH in a D_2O aqueous solution and 50 mM CTAB micelle samples. Micelle samples were referenced with internal DSS standard at 0.000 ppm and aqueous stock samples were referenced with external DSS/D_2O at 0.000 ppm.

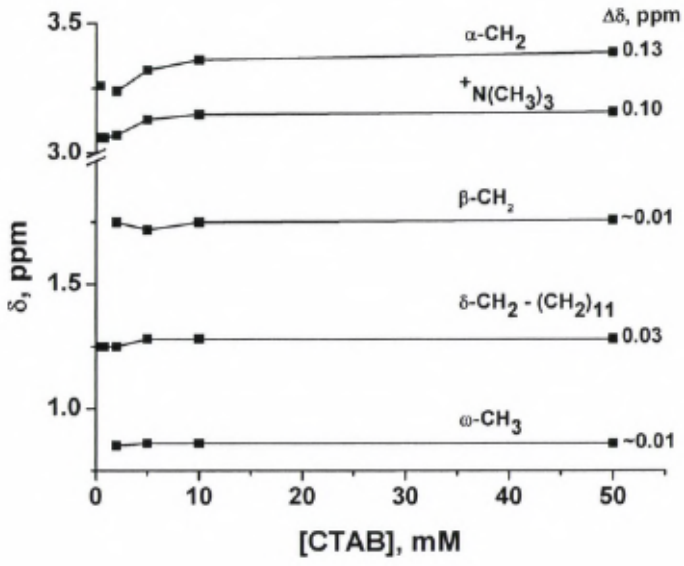

(a)

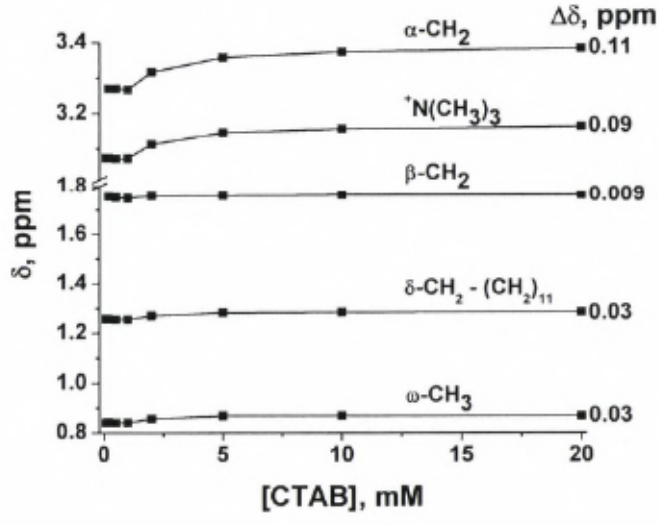

(b)

Figure 12: Comparison of CTAB chemical shifts vs. CTAB concentration with and without $[VO_2(ma)_2]^-$. The CTAB peaks were all referenced with deuterated benezene and TMS. The TMS peak was set to 0.000 ppm and benezene was stationary throughout all the samples at 7.16 ppm. The values in brackets on the far right of the graph represent the difference in chemical shifts as the CTAB concentration was varied. (a) $\Delta\delta$, ppm = $\delta_{50\text{ mM CTAB}} - \delta_{0.04\text{ mM CTAB}}$. CTAB micelle samples were all adjusted to a pH value of 9 and were analyzed at 35°C. (b) $\Delta\delta$, ppm = $\delta_{20\text{ mM CTAB}} - \delta_{0.01\text{ mM CTAB}}$; samples were analyzed at 35°C; data was recorded and graph was generated by Dr. Ernestas Gaidamauskas, in review. The graph was modified for comparison for this work.

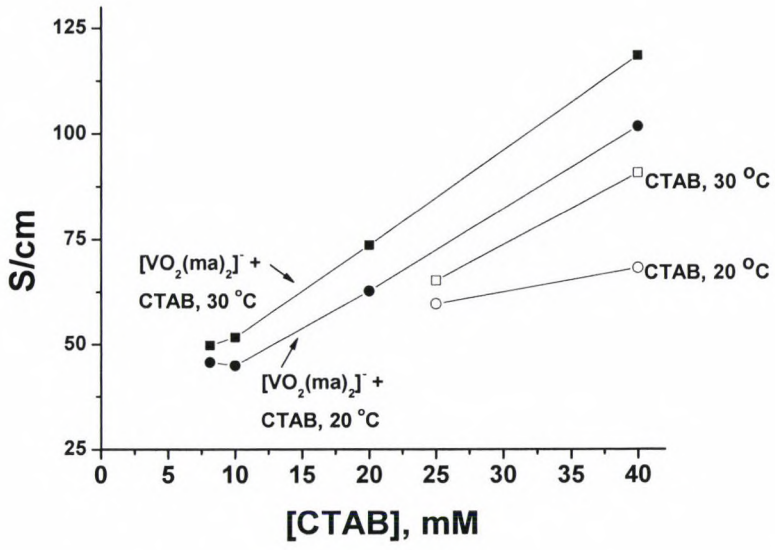

Figure 13: Comparison of CTAB micelle conductance above the *cmc* and above/below the T_k. 20 mM $[VO_2(ma)_2]^-$ aqueous stock was used to make samples and a total concentration of 2 mM of $[VO_2(ma)_2]^-$ was held constant as the CTAB concentration was varied.

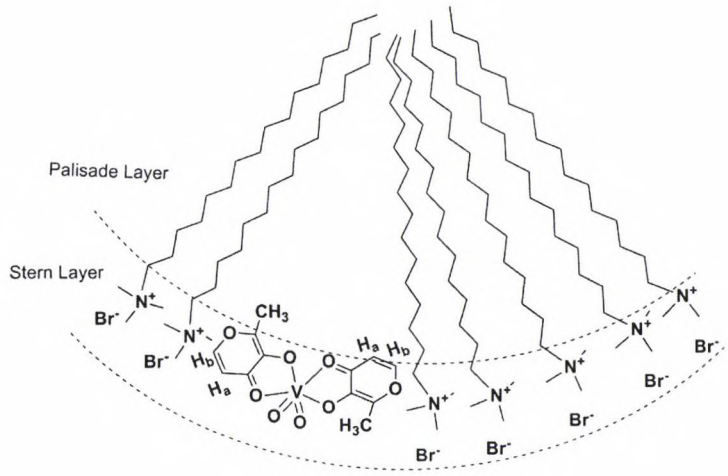

(a)

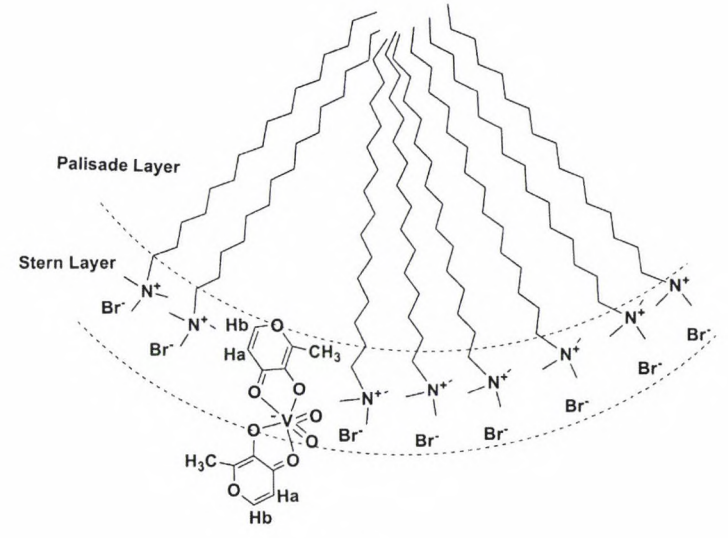

(b)

Figure 14: Two proposed hypotheses of $[VO_2(ma)_2]^-$ penetration into the polar region of the CTAB micelle interface. (a) shows entire $[VO_2(ma)_2]^-$ in stern layer; (b) shows partial penetration of $[VO_2(ma)_2]^-$ into interface.

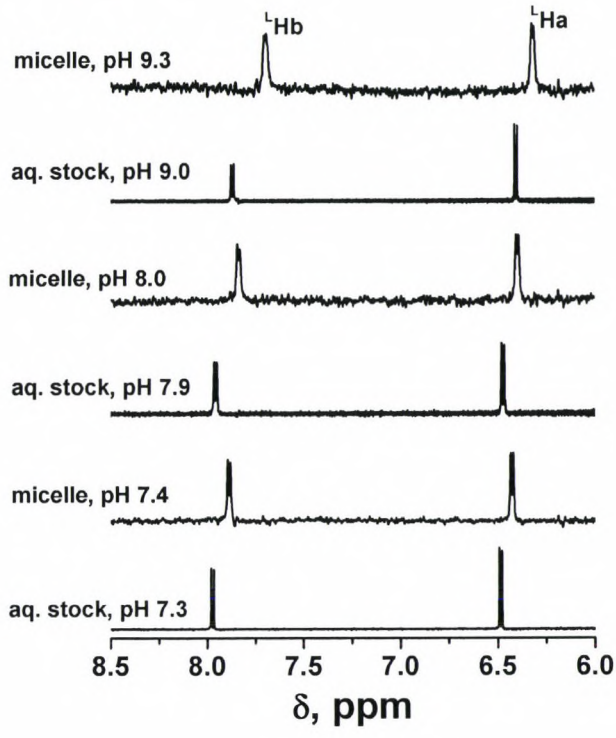

Figure 15: ^{1}H NMR spectra showing chemical shifts of maltol protons comparing aqueous with micelles. Samples were prepared from 4 mM maltol in D_2O and 50 mM CTAB and are at pH values of 7, 8 and 9.

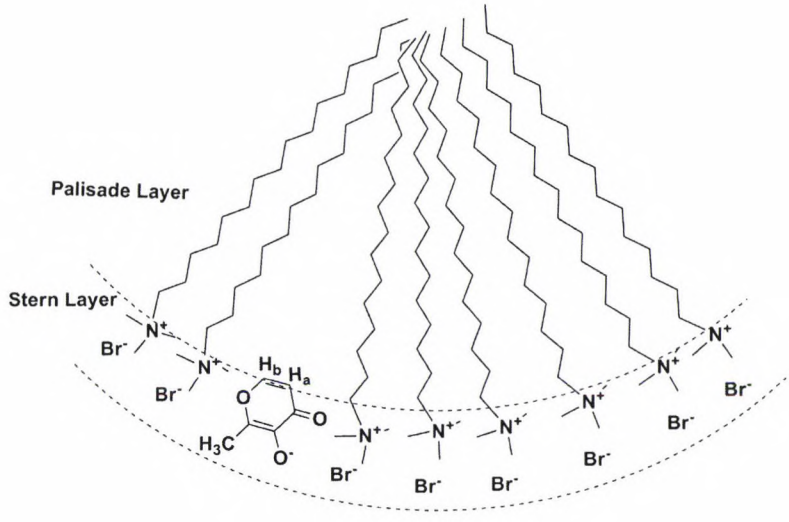

(a)

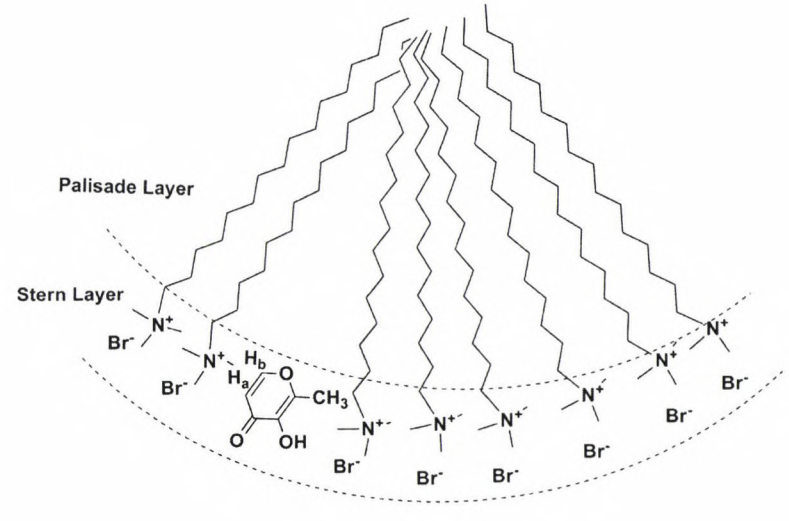

(b)

Figure 16: Two proposed possibilities of maltol penetration into stern layer of the micelle. (a) Deprotonated form of maltol and its level of penetration. (b) Protonated form of maltol and its penetration into the micelle.

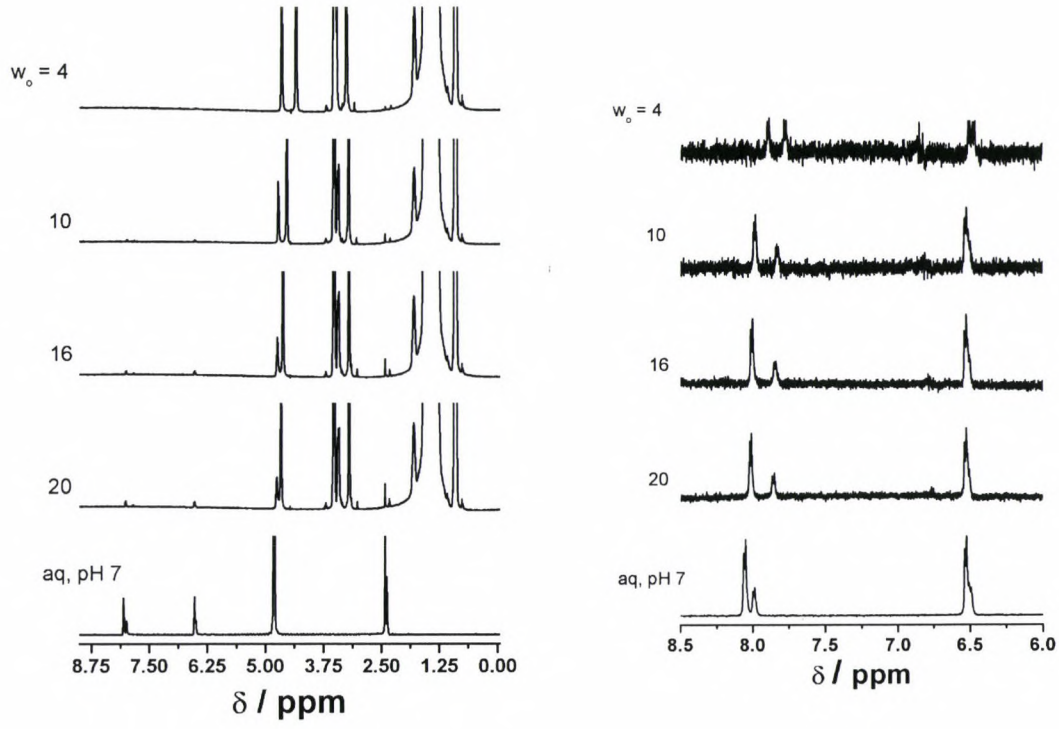

Figure 17: ^{1}H NMR spectra of RM samples with varying w_o size at pH 7 (left). Samples were prepared from 100 mM $[VO_2(ma)_2]^-$ and 200 mM CTAB. (right) ^{1}H NMR insert of RM samples with varying w_o size at pH 7 focusing on the complex and free maltol signals. RM samples were referenced using internal C_6H_{12} which was referenced to 1.44 ppm. Aqueous samples were referenced externally using a different NMR tube that contained DSS/D_2O (0.000 ppm).

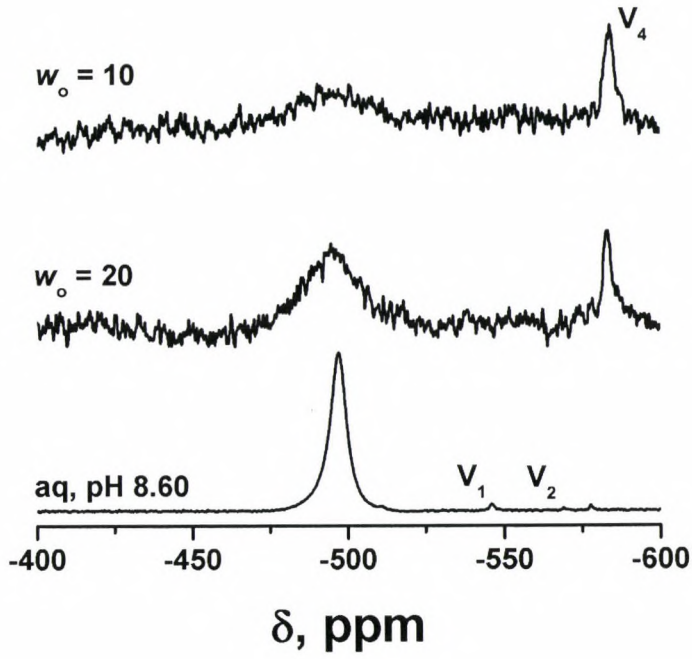

Figure 18: ^{51}V NMR spectra of a 100 mM CTAB/1-pentanol/cyclohexane/D_2O RM sample containing 100 mM $[VO_2(ma)_2]^-$ in D_2O at pH 8.6.

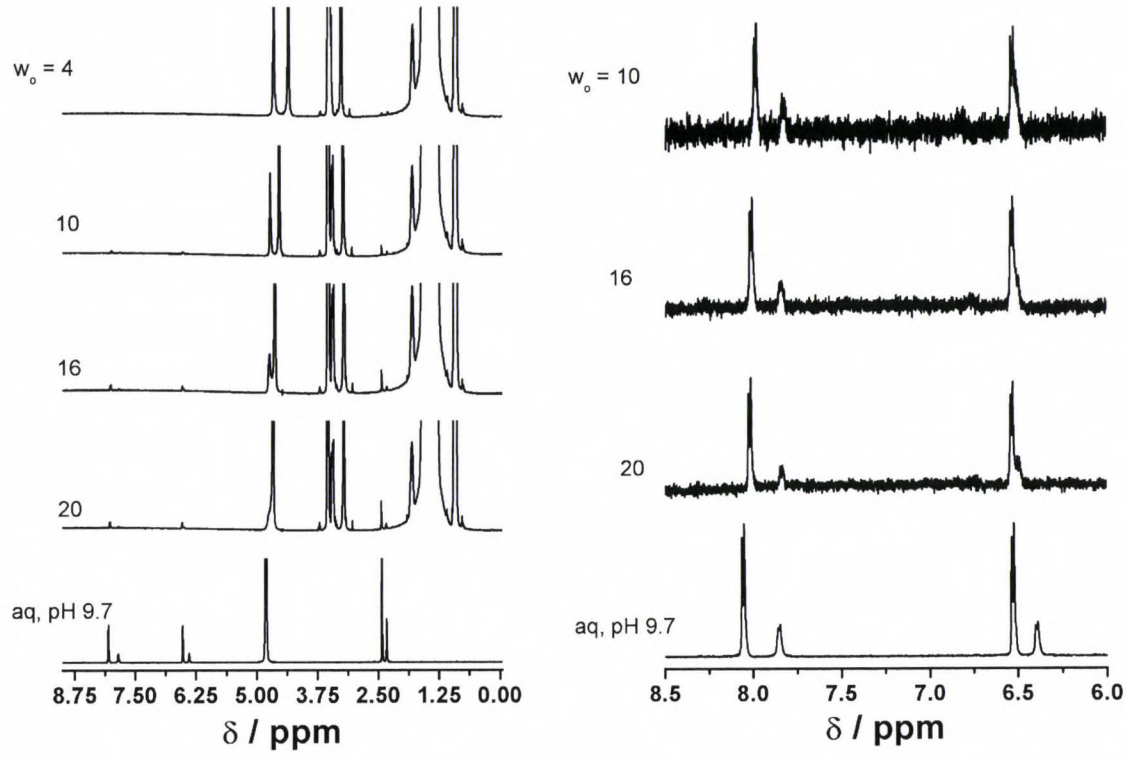

Figure 19: ^{1}H NMR spectra showing 200 mM CTAB/1-pentanol/cyclohexane/D_2O RMs at pH 9.7. Samples contained 100 mM $[VO_2(ma)_2]^-$ (left). (right) insert of the NMR spectra 6.0 to 8.5 ppm from the spectra shown focusing on the protons located on complex and free maltol ligand. The aqueous samples were referenced externally using a different NMR tube containing DSS/D_2O (0.000 ppm) and RM samples were referenced using internal C_6H_{12} at 1.44 ppm.

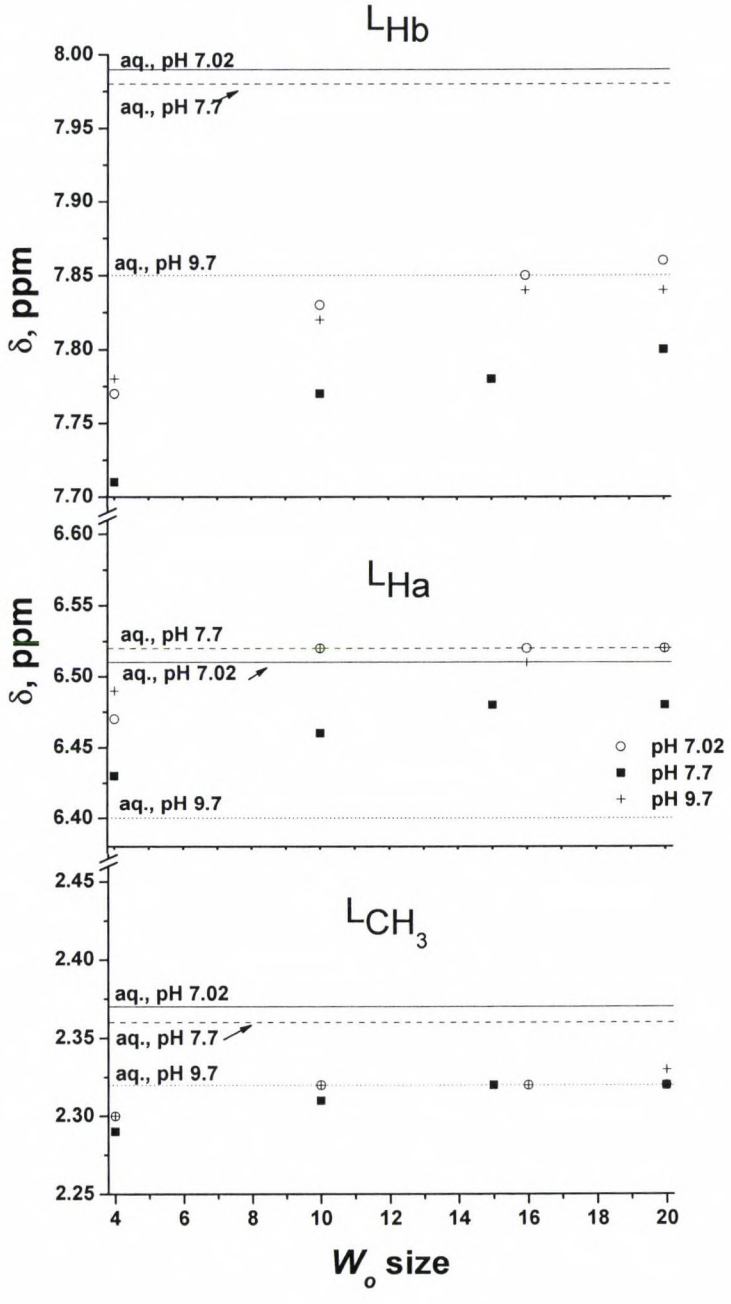

Figure 20: Chemical shifts of H_a, H_b and CH_3 for maltol in the presence of $[VO_2(ma)_2]^-$. Signals for maltol in 200 mM CTAB RMs at pH values of approximately 7, 8, and 9.7. The RM samples were referenced using internal C_6H_{12} at 1.44 ppm. Maltol and D_2O sample was referenced using an external NMR tube that contained DSS and D_2O, referenced to 0.000 ppm.

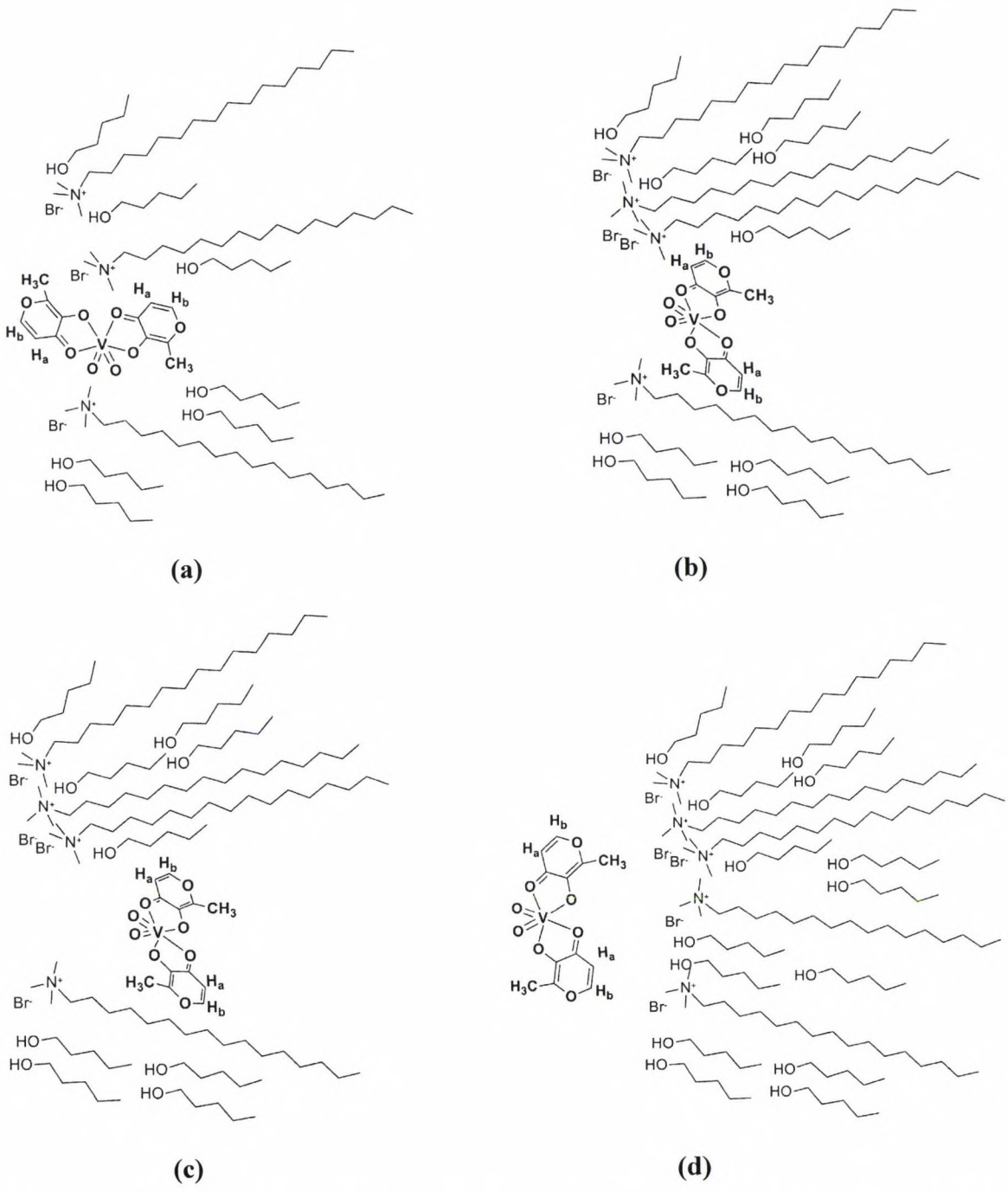

Figure 21: Four proposed models of $[VO_2(ma)_2]^-$ interaction with the CTAB RM system based on interpretation of multinuclear NMR techniques. Half of the complex is penetrating (a); complex is interacting with polar head group (b); complex is completely in non-polar region (c); and complex is remaining in bulk water until the w_o size restricts its movement (d).

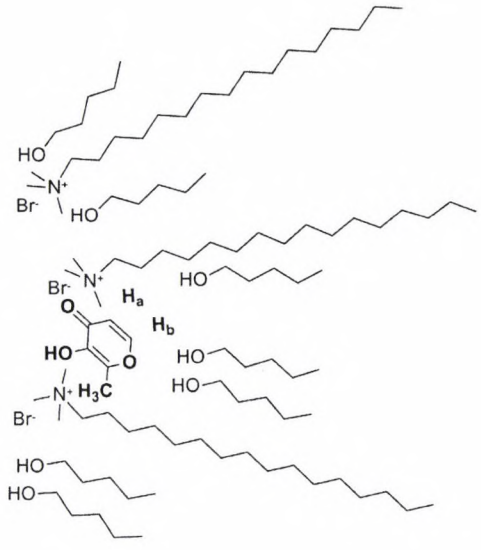

Figure 22: A proposed model for maltol location in CTAB/1-pentanol/cyclohexane/ D_2O RM interface.

CHAPTER III

CONCLUSIONS AND FUTURE PLANS

Conclusions

Based on multinuclear NMR results on two model membrane systems, micelles and reverse micelles and using a cationic surfactant to represent the phosphatidylcholine head group found within cellular membranes, we hypothesize that a negatively charged oxovanadium(V) compound $[VO_2(ma)_2]^-$ penetrates into the positively charged interface of these model membranes. The complex does not shift on aqueous solution NMR spectra as a function of pH. However, when the complex is placed in a micellar solution, an upfield chemical shift is observed for all protons located on the complex. Therefore, the environment that the protons are located in must be different from that in aqueous solution. In addition, experiments with CTAB RM systems enabled us to demonstrate that, although there is slight shifting in the protons as the w_o size of the RM decreased, there was still a chemical shift. This suggests that the complex is interacting with RM weakly. A similar observation was made from ^{51}V NMR spectroscopy obtained as a function of w_o size and agree with other literature studies. Free maltol ligand is a much more difficult compound to work with due to its tendency to undergo changes in charge as a function of pH. Therefore, upfield chemical shifting can be the result of either deprotonation or penetration and careful studies that examine the effect of maltol on these systems at very high pH values should be performed. For micelles, we concluded that

protonated or deprotonated maltol penetrates into the polar region of CTAB. However, slight changes in the proton locations on maltol are observed.

To complete these studies, it would be worthwhile to examine maltol without any complex in CTAB micelles as a function of CTAB concentration. This study would clarify whether free maltol interacts with the micelle in the absence of a complex. It is predicted that maltol will cause a change in CTAB chemical shifts above the *cmc*. In addition, conductivity studies should examine samples that are below the *cmc* to verify with literature values. It is predicted that there will be a very noticeable change in conductance both below and above the *cmc* and above it. A more thorough interpretation comparing chemical shifts of the drug of interest in micelles and reverse micelles will also provide a better understanding of exact location of complex and maltol in these systems (Figures 23 and 24).

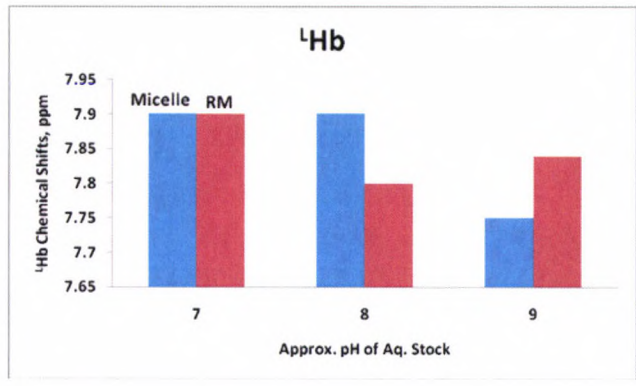

(a)

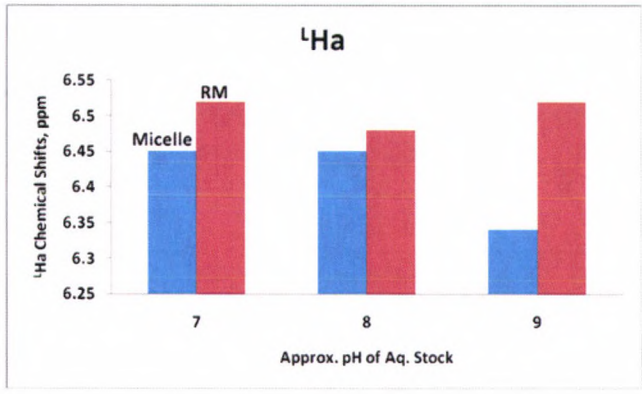

(b)

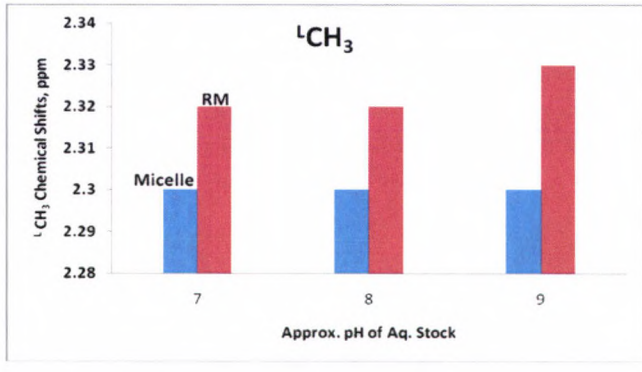

(c)

Figure 23: Chemical shifts of the hydrolyzed product of $[VO_2(ma)_2]^-$, maltol in RM and micelle systems. 100 mM and 2 mM of $[VO_2(ma)_2]^-$ were used in RM and micelle solutions, respectively.

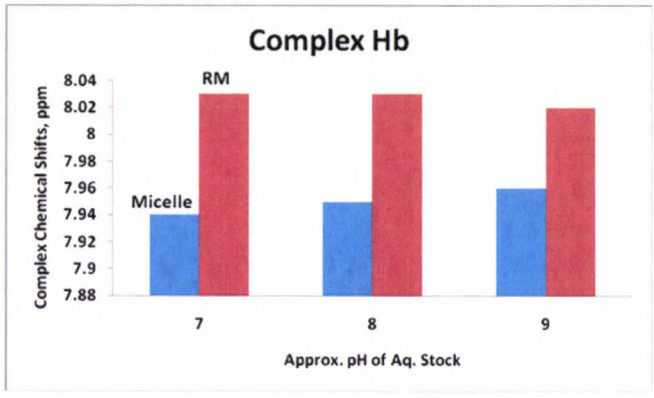

(a)

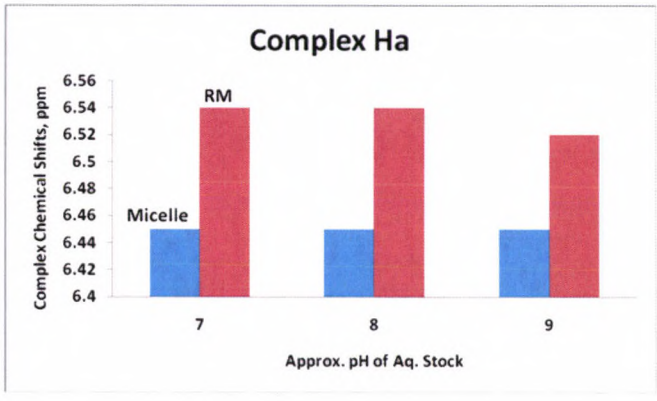

(b)

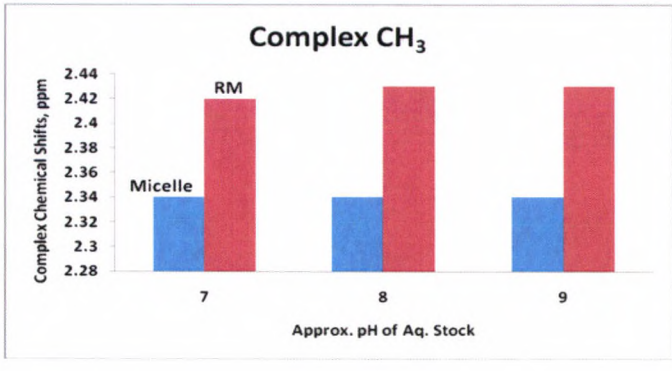

(c)

Figure 24: Chemical shifts of $[VO_2(ma)_2]^-$ in RM and micelle system. 2 mM and 100 mM $[VO_2(ma)_2]^-$ in micelle and RM samples, respectively.

REFERENCES

1. Thompson, K. H., and C. Orvig. 2000. Design of vanadium compounds as insulin enhancing agents. *Journal of the Chemical Society-Dalton Transactions*: 2885-2892.

2. Brichard, S. M., and J. C. Henquin. 1995. The Role of Vanadium in the Management of Diabetes. *Trends in Pharmacological Sciences* **16**: 265-270.

3. Pepato, M. T., N. M. Khalil, M. P. Giocondo, and I. L. Brunetti. 2008. Vanadium and its complexes: The renewed interest in its biochemistry. *Latin American Journal of Pharmacy* **27**: 468-476.

4. Sakurai, H., A. Katoh, and Y. Yoshikawa. 2006. Chemistry and biochemistry of insulin-mimetic vanadium and zinc complexes. Trial for treatment of diabetes mellitus. *Bulletin of the Chemical Society of Japan* **79**: 1645-1664.

5. Bortolini, O., and V. Conte. 2005. Vanadium (V) peroxocomplexes: Structure, chemistry and biological implications. *Journal of Inorganic Biochemistry* **99**: 1549-1557.

6. Crans, D. C., J. J. smee, E. Gaidamauskas, and L. Yang. 2004. The Chemistry and Biochemistry of Vanadium and the Biological Activities Exerted by Vanadium Compounds. *Chemical Reviews* **104**: 849-902.

7. Heidari, Z., H. Mahmoudzadeh-Sagheb, and B. Moudi. 2008. A quantitative study of sodium tungstate protective effect on pancreatic beta cells in streptozotocin-induced diabetic rats. *Micron* **39**: 1300-1305.

8. Thompson, K. H., and C. Orvig. 2004. Vanadium compounds in the treatment of diabetes. *Metal Ions in Biological Systems, Vol 41: Metal Ions and Their Complexes in Medication* **41**: 221-252.

9. Cam, M. C., B. Rodrigues, and J. H. McNeill. 1999. Distinct glucose lowering and beta cell protective effects of vanadium and food restriction in streptozotocin-diabetes. *European Journal of Endocrinology* **141**: 546-554.

10. Srivastava, A. K., and M. Z. Mehdi. 2005. Insulino-mimetic and anti-diabetic effects of vanadium compounds. *Diabetic Medicine* **22**: 2-13.

11. Sekar, N., J. P. Li, and Y. Shechter. 1996. Vanadium salts as insulin substitutes: Mechanisms of action, a scientific and therapeutic tool in diabetes mellitus research. *Critical Reviews in Biochemistry and Molecular Biology* **31**: 339-359.

12. Sakurai, H. 2008. Treatment of diabetes in experimental animals by metallocomplexes. *Yakugaku Zasshi-Journal of the Pharmaceutical Society of Japan* **128**: 317-322.

13. Kiss, T., T. Jakusch, D. Hollender, A. Dornyei, E. A. Enyedy, J. C. Pessoa, H. Sakurai, and A. Sanz-Medel. 2008. Biospeciation of antidiabetic VO(IV) complexes. *Coordination Chemistry Reviews* **252**: 1153-1162.

14. Goc, A. 2006. Biological activity of vanadium compounds. *Central European Journal of Biology* **1**: 314-332.

15. Thompson, K. H., and C. Orvig. 2006. Vanadium in diabetes: 100 years from Phase 0 to Phase I. *Journal of Inorganic Biochemistry* **100**: 1925-1935.

16. Rehder, D. 2003. Biological and medicinal aspects of vanadium. *Inorganic Chemistry Communications* **6**: 604-617.

17. Cam, M. C., R. W. Brownsey, and J. H. McNeill. 2000. Mechanisms of vanadium action: insulin-mimetic or insulin-enhancing agent? *Canadian Journal of Physiology and Pharmacology* **78**: 829-847.

18. Goldfine, A. B., M. E. Patti, L. Zuberi, B. J. Goldstein, R. LeBlanc, E. J. Landaker, Z. Y. Jiang, G. R. Willsky, and C. R. Kahn. 2000. Metabolic effects of vanadyl sulfate in humans with non-insulin-dependent diabetes mellitus: In vivo and in vitro studies. *Metabolism-Clinical and Experimental* **49**: 400-410.

19. Buglyo, P., D. C. Crans, E. M. Nagy, R. L. Lindo, L. Q. Yang, J. J. Smee, W. Z. Jin, L. H. Chi, M. E. Godzala, and G. R. Willsky. 2005. Aqueous chemistry of the vanadium(III) (V-III) and the V-III-dipicolinate systems and a comparison of the effect of three oxidation states of vanadium compounds on diabetic hyperglycemia in rats. *Inorganic Chemistry* **44**: 5416-5427.

20. Crans, D. C., A. D. Keramidas, and C. Drouza. 1996. Organic Vanadium Compounds - Transition State Analogy with Organic Phosphorous Compounds. *Phosphorous, Sulfur, and Silicon* **109-110**: 245-248.

21. Aureliano, M., and D. C. Crans. 2009. Decavanadate () and oxovanadates: Oxometalates with many biological activities. *Journal of Inorganic Biochemistry* **103**: 536-546.

22. Crans, D. C., M. Tahir-Mahroof, O. P. Anderson, and M. M. Miller. 1994. X-ray structure of (NH4)6(Gly-Gly)2V10028*4H2O: Model Structures for Polyoxometalate-Protein Interactions. *Inorganic Chemistry* **33**: 5586-5590.

23. Baruah, B., J. Roden, M. Sedgwick, M. N. Correa, D. C. Crans, and N. E. Levinger. 2006. When is water not water? Exploring water confined in large reverse micelles using a highly charged inorganic molecular probe. *Journal of the American Chemical Society* **128**: 12758-12765.

24. Thompson, K. H., and C. Orvig. 2001. Coordination chemistry of vanadium in metallopharmaceutical candidate compounds. *Coordination Chemistry Reviews* **219**: 1033-1053.

25. Crans, D. C., and J. J. Smee. 2003. 4.4 Vanadium. *Comprehensive Coordination Chemistry II* **4**: 175-239.

26. Crans, D. C. 2000. Chemistry and insulin-like properties of vanadium(IV) and vanadium(V) compounds. *Journal of Inorganic Biochemistry* **80**: 123-131.

27. McNeill, J. H., V. G. Yuen, H. R. Hoveyda, and C. Orvig. 1992. Bis(maltolato)oxovanadium(IV) is a potent insulin mimetic. *J. Med. Chem.* **35**: 1489.

28. Sakurai, H., Y. Kojima, Y. Yoshikawa, K. Kawabe, and H. Yasui. 2002. Antidiabetic vanadium(IV) and zinc(II) complexes. *Coordination Chemistry Reviews* **226**: 187-198.

29. Sakurai, H., and H. Yasui. 2003. Structure-activity relationship of insulinomimetic vanadyl-picolinate complexes in view of their clinical use. *Journal of Trace Elements in Experimental Medicine* **16**: 269-280.

30. Thompson, K. H., J. Lichter, C. LeBel, M. C. Scaife, J. H. McNeill, and C. Orvig. 2009. Vanadium treatment of type 2 diabetes: A view to the future. *Journal of Inorganic Biochemistry* **103**: 554-558.

31. Brautigan, D. L., A. Kruszewski, and H. Wang. 2006. Chromium and vanadate combination increases insulin-induced glucose uptake by 3T3-L1 adipocytes. *Biochemical and Biophysical Research Communications* **347**: 769-773.

32. Krejsa, C. M., S. G. Nadler, J. M. Esselstyn, T. J. Kavanagh, J. A. Ledbetter, and G. L. Schieven. 1997. Role of oxidative stress in the action of vanadium phosphotyrosine phosphatase inhibitors - Redox independent activation of NF-kappa B. *Journal of Biological Chemistry* **272**: 11542-11549.

33. Bevan, A. P., P. G. Drake, J. F. Yale, A. Shaver, and B. I. Posner. 1995. Peroxovanadium compounds: Biological actions and mechanism of insulin-mimesis. *Molecular and Cellular Biochemistry* **153**: 49-58.

34. Posner, B. I., R. Faure, J. W. Burgess, A. P. Bevan, D. Lachance, G. Zhang-Sun, G. I. Fantus, J. B. Ng, D. A. Hall, B. S. Lum, and A. Shaver. 1994. Peroxovanadium Compounds. A new class of potent phosphotyrosine phosphatase inhibitors which are insulin mimetics. *The Journal of Biological Chemistry* **269**: 4596-4604.

35. Lopez, V., T. Stevens, and R. N. Lindquist. 1976. Vanadium Ion Inhibition of Alkaline Phosphatase-Catalyzed Phosphate Ester Hydrolysis. *Archives of Biochemistry and Biophysics* **175**: 31-38.

36. Bevan, A. P., P. G. Drake, J. F. Yale, A. Shaver, and B. I. Posner. 1995. Peroxovanadium compounds: Biological actions and mechanism of insulin-mimesis. *Molecular and Cellular Biochemistry* **153**: 49-58.

37. Marzban, L., R. Rahimian, R. W. Brownsey, and J. H. McNeill. 2002. Mechanisms by which Bis(Maltolato)Oxovanadium(IV) Normalizes Phosphoenolpyruvate Carboxykinase and Glucose-6-Phosphatase Expression in Streptozotocin-Diabetic Rats *in Vivo*. *Endocrinology* **143**: 4636-4645.

38. Sakurai, H. 2007. Structure-Activity Relationship and Molecular Action Mechanism in the Family of Antidiabetic *bis*(Picolinato)oxovanadium(IV) Complexes.

39. Li, M., J. J. Smee, W. Ding, and D. C. Crans. 2009. Anti-diabetic effects of sodium 4-amino-2,6-dipicolinatodioxovanadium(V) dihydrate in streptozotocin-induced diabetic rats. *Journal of Inorganic Biochemistry* **103**: 585-589.

40. Huyer, G., S. Liu, J. Kelly, J. Moffat, P. Payette, B. Kennedy, G. Tsaprailis, M. J. Gresser, and C. Ramachandran. 1997. Mechanisms of Inhibition of Protein-tyrosine Phosphatases by Vanadate and Pervanadate. *Journal of Biological Chemistry* **272**: 843-851.

41. Goldstein, B. J. 2002. Protein-Tyrosine Phosphatases: Emerging Targets for Therapeutic Intervention in Type 2 Diabetes and Related States of Insulin Resistance. *The Journal of Clinical Endocrinology and Metabolism* **87**: 2474-2480.

42. Hulley, P., and A. Davison. 2003. Regulation of tyrosine phosphorylation cascades by phosphatases: What the actions of vanadium teach us. *Journal of Trace Elements in Experimental Medicine* **16**: 281-290.

43. Bleyle, L. A., Y. Peng, C. Ellis, and R. A. Mooney. 1999. Dissociation of PTPase Levels from Their Modulation of Insulin Receptor Signal Transduction. *Cell. Signal.* **11**: 719-725.

44. Tracey, A. S., G. R. Willsky, and E. S. Takeuchi. 2007. The Influence of Vanadium Compounds on Biological Systems. *In* Vanadium: Chemistry, Biochemistry, Pharmacology and Practical Applications. CRC Press
Taylor & Francis Group, Boca Raton. 196.

45. Shaver, A., J. B. Ng, D. A. Hall, and B. I. Posner. 1995. The chemistry of peroxovanadium compounds relevant to insulin mimesis. *Molecular and Cellular Biochemistry* **153**: 5-15.

46. Winter, C. L., J. S. Lange, M. G. Davis, G. S. Gerwe, T. R. Downs, K. G. Peters, and B. Kasibhatla. 2005. A nonspecific phosphotyrosine phosphatase inhibitor, bis(maltolato)oxovanadium(IV), improves glucose tolerance and prevents diabetes in Zucker diabetic fatty rats. *Experimental Biology and Medicine* **230**: 207-216.

47. Pugazhenthi, S., F. Tanha, B. Dahl, and R. L. Khandelwal. 1995. Decrease in protein tyrosine phosphatase activities in vanadate-treated obese Zucker (fa/fa) rat liver. *Molecular and Cellular Biochemistry* **153**: 125-129.

48. Shisheva, A., O. Ikonomov, and Y. Shechter. 1994. The Protein-Tyrosine-Phosphatase Inhibitor, Pervanadate, Is a Powerful Antidiabetic Agent in Streptozotocin-Treated Diabetic Rats. *Endocrinology* **134**: 507-510.

49. Fantus, I. G., G. Deragon, R. Lai, and S. Tang. 1995. Modulation of insulin action by vanadate: Evidence of a role for phosphotyrosine phosphatase activity to alter cellular signaling. *Molecular and Cellular Biochemistry* **153**: 103-112.

50. Kennedy, B., and C. Ramachandran. 2000. Protein Tyrosine Phosphatase-1B in Diabetes. *Biochemical Pharmacology* **60**: 877-883.

51. Melchior, M., S. J. Rettig, B. D. Liboiron, K. H. Thompson, V. G. Yuen, J. H. McNeill, and C. Orvig. 2001. Insulin-Enhancing Vanadium(III) Complexes. *Inorganic Chemistry* **40**: 4686-4690.

52. Brand, R. M., and F. G. Hamel. 1999. Transdermally delivered peroxovanadium can lower blood glucose levels in diabetic rats. *International Journal of Pharmaceutics* **183**: 117-123.

53. Cros, G., J. J. Mongold, J. J. Serrano, S. Ramanadham, and J. H. Mcneill. 1992. Effects of Vanadyl Derivatives on Animal-Models of Diabetes. *Molecular and Cellular Biochemistry* **109**: 163-166.

54. Willsky, G. R., L. H. Chi, Y. L. Liang, D. P. Gaile, Z. H. Hu, and D. C. Crans. 2006. Diabetes-altered gene expression in rat skeletal muscle corrected by oral administration of vanadyl sulfate. *Physiological Genomics* **26**: 192-201.

55. Hiromura, M., Y. Adachi, M. Machida, M. Hattori, and H. Sakurai. 2009. Glucose lowering activity by oral administration of bis(allixinato)oxidovanadium(IV) complex in streptozotocin-induced diabetic mice and gene expression profiling in their skeletal muscles. *Metallomics* **1**: 92-100.

56. Valera, A., J. E. Rodriguez-Gill, and F. Bosch. 1993. Vanadate Treatment Restores the Expression of Genes for Key Enzymes in the Glucose and Ketone Bodies Metabolism in the Liver of Diabetic Rats. *Journal of Clinical Investigations* **92**: 4-11.

57. Brichard, S. M., L. N. Ongemba, J. Girard, and J. C. Henquin. 1994. Tissue-specific correction of lipogenic enzyme gene expression in diabetic rats given vanadate. *Diabetologia* **37**: 1065-1072.

58. Wei, D., M. Li, and W. Ding. 2007. Effect of vanadate on gene expression of the insulin signaling pathway in skeletal muscle of streptozotocin-induced diabetic rats. *Journal of Biological Inorganic Chemistry* **12**: 1265-1273.

59. Brichard, S. M., B. Desbuquois, and J. Girard. 1993. Vanadate Treatment of Diabetic Rats Reverses the Impaired Expression of Genes Involved in Hepatic Glucose-Metabolism - Effects on Glycolytic and Gluconeogenic Enzymes, and on Glucose Transporter Glut2. *Molecular and Cellular Endocrinology* **91**: 91-97.

60. Brichard, S. M. 1995. Effects of vanadate on the expression of genes involved in fuel homeostasis in animal models of Type I and Type II diabetes. *Molecular and Cellular Biochemistry* **153**: 121-124.

61. Yang, X. G., X. D. Yang, L. Yuan, K. Wang, and D. C. Crans. 2004. The permeability and cytotoxicity of insulin-mimetic vanadium compounds. *Pharmaceutical Research* **21**: 1026-1033.

62. Ramos, S., M. Manuel, T. Tiago, R. Duarte, J. Martins, C. Gutierrz-Merino, J. J. G. Moura, and M. Aureliano. 2006. Decavanadate interactions with actin: Inhibition of G-actin poymerization and stabilization of decameric vanadate. *Journal of Inorganic Biochemistry* **100**: 1734-1743.

63. Ramos, S., R. O. Duarte, J. J. G. Moura, and M. Aureliano. 2009. Decavanadate interactions with actin: cysteine oxidation and vanadyl formation. *Dalton Transactions*: 7985-7994.

64. Combeau, C., and M. F. Carlier. 1988. Probing the Mechanism of ATP hydrolysis on F-actin using Vanadate and the Structural Analogs of Phosphate BeF3- and AIF4-*. *The Journal of Biological Chemistry* **263**: 17429-17436.

65. Chesarone, M. A., and B. L. Goode. 2009. Actin nucleation and elongation factors: mechanisms and interplay. *Current Opinions in Cell Biology* **21**: 28-37.

66. Alberts, B., A. Johnson, J. Lewis, M. Raff, K. Roberts, and P. Walter. 2007. Molecular Biology of the Cell. 5 ed. Garland Science
Taylor & Francis Group, LLC, New York.

67. Pollard, T. D., and G. G. Borisy. 2003. Cellular Motility Driven by Assembly and Disassembly of Actin Filaments. *Cell* **112**: 453-465.

68. Remedios, C. G. D., D. Chhabra, M. Kekic, V. I. Dedova, M. Tsubakihara, D. A. Berry, and N. J. Nosworthy. 2003. Actin Binding Proteins: Regulation of cytoskeletal microfilaments. *Physiology Review* **83**: 433-473.

69. Pereira, M. J., E. Carvalho, J. W. Eriksson, D. C. Crans, and M. Aureliano. 2009. Effects of decavanadate and insulin enhancing vanadium compounds on glucose uptake in isolated rat adipocytes. *Journal of Inorganic Biochemistry* **103**: 1687-1692.

70. Brener, E., S. Rubinstein, G. Cohen, K. Shternall, J. Rivlin, and H. Breitbart. 2003. Remodeling of the Actin Cytoskeleton During Mammalian Sperm Capacitation and Acrosome Reaction. *Biology of Reproduction* **68**: 837-845.

71. Goodno, C. C., and E. W. Taylor. 1982. Inhibition of actomyosin ATPase by vanadate. *Biochemistry* **79**: 21-25.

72. Rivadeneira, J., D. A. Barrio, G. Arrambide, D. Gambino, L. Bruzzone, and S. B. Etcheverry. 2009. Biological effects of a complex of vanadium(V) with salicylaldehyde semicarbazone in osteoblasts in culture: Mechanism of action. *Journal of Inorganic Biochemistry* **103**: 633-642.

73. Osinska-Krolicka, I., H. Podsiadly, K. Bukietynska, M. Zemanek-Zboch, D. Nowak, K. Suchoszek-Lukaniuk, and M. Malicka-Blaszkiewics. 2004. Vanadium(III) complexes with L-cysteine - stability, speciation and the effect on actin in hepatoma Morris 5123 cells. *Journal of Inorganic Biochemistry* **98**: 2087-2098.

74. Coulombe, P. A., and P. Wong. 2004. Cytoplasmic intermediate filaments revealed as dynamic and multipurpose scaffolds. *Nature Cell Biology* **6**: 699-706.

75. Strnad, P., R. Windoffer, and R. E. Leube. 2003. Light-induced Resistance of the Keratin Network to the Filament-disrupting Tyrosine Phosphatase Inhibitor Orthovanadate. *The Journal of Investigative Dermatology* **120**: 198-203.

76. Omary, M. B., P. A. Coulombe, and W. H. I. McLean. 2004. Mechanisms of Disease: Intermediate Filament Protein and Their Associated Diseases. *The New England Journal of Medicine* **351**: 2087-2100.

77. Woll, S., R. Windoffer, and R. E. Leube. 2007. p38 MAPK-dependent shaping of the keratin cytoskeleton in cultured cells. *The Journal of Cell Biology* **177**: 795-807.

78. Godsel, L. M., R. P. Hobbs, and K. J. Green. 2008. Intermediate filament assembly: dynamics to disease. *Trends in Cellular Biology* **18**: 28-37.

79. Kirazov, E. P., and D. G. Weiss. 1986. Effects of Vanadate on the Assembly and Disassembly of Purified Tubulin. *Cell Motility and the Cytoskeleton* **6**: 314-323.

80. Kaplan, J. H. 2002. Biochemistry of Na,K-ATPase. *Annual Reviews in Biochemistry* **71**: 511-535.

81. Lutsenko, S., and J. H. Kaplan. 1995. Organization of P-Type ATPases: Significance of Structural Diversity. *Biochemistry* **34**: 15607-15613.

82. Axelsen, K. B., and M. G. Palmgren. 1998. Evolution of Substrate Specificities in the P-Type ATPase Superfamily. *Journal of Molecular Evolution* **46**: 84-101.

83. Kasamo, K. 2003. Regulation of plasma membrane H+-ATPase activity by the membrane environment. *Journal of Plant Research* **116**: 517-523.

84. Mahaney, J. E., J. Kleinschmidt, D. Marsh, and D. D. Thomas. 1992. Effects of melittin on lipid-protein interactions in sarcoplasmic reticulum membranes. *Biophysical Journal* **63**: 1513-1522.

85. Mangialavori, I., A. M. Giraldo, C. M. Buslje, M. F. Gomes, A. J. Caride, and J. P. Rossi. 2009. A New Conformation in Sarcoplasmic Reticulum Calcium Pump and Plasma Membrane Ca++ Pumps Revealed by a Photoactivatable Phospholipidic Probe. *The Journal of Biological Chemistry* **284**: 4823-4828.

86. Toustrup-Jensen, M., and B. Vilsen. 2003. Importance of Conserved Thr214 in Domain A of the Na+,K+-ATPase for Stabilization of the Phosphoryl Transition State Complex in E2P Dephosphorylation. *The Journal of Biological Chemistry* **278**: 11402-11410.

87. Clausen, J. D., D. B. McIntosh, D. G. Woolley, A. N. Anthonisen, B. Vilsen, and J. P. Andersen. 2006. Asparagine 706 and Glutamate 183 at the Catalytic Site of Sarcoplasmic Reticulum Ca++-ATPase Play Critical but Distinct Roles in E2 States. *The Journal of Biological Chemistry* **281**: 9471-9481.

88. Kwong, D. W. J., W. N. Leung, M. Xu, S. Q. Zhu, and C. H. K. Cheng. 1996. Modulatory Effects of Peroxovanadates on Insulin Receptor Binding. *Journal of Inorganic Biochemistry* **64**: 163-180.

89. Elberg, G., J. Li, and Y. Shechter. 1994. Vanadium activates or inhibits receptor and non-receptor protein tyrosine kinases in cell-free experiments, depending on its oxidation state. Possible role of endogenous vanadium in controlling cellular protein tyrosine kinase activity. *Journal of Biological Chemistry.* **269**: 9521-9527.

90. Mehdi, M. Z., S. K. Pandey, J. F. Theberge, and A. K. Srivastava. 2006. Insulin signal mimicry as a mechanism for the insulin-like effects of vanadium. *Cell Biochemistry and Biophysics* **44**: 73-81.

91. Basuki, W., M. Hiromura, Y. Adachi, K. Tayama, M. Hattori, and H. Sakurai. 2006. Enhancement of insulin signaling pathway in adipocytes by oxovanadium(IV) complexes. *Biochemical and Biophysical Research Communications* **349**: 1163-1170.

92. Kawabe, K., Y. Yoshikawa, Y. Adachi, and H. Sakurai. 2006. Possible mode of action for insulinomimetic activity of vanadyl(IV) compounds in adipocytes. *Life Sciences* **78**: 2860-2866.

93. Hiromura, M., A. Nakayama, Y. Adachi, M. Doi, and H. Sakurai. 2007. Action mechanism of bis(allixinato)oxovanadium(IV) as a novel potent insulin-mimetic complex: regulation of GLUT4 translocation and FoxO1 transcription factor. *Journal of Biological Inorganic Chemistry* **12**: 1275-1287.

94. Goldwaser, I., J. P. Li, E. Gershonov, M. Armoni, E. Karnieli, M. Fridkin, and Y. Shechter. 1999. L-glutamic acid gamma-monohydroxamate - A potentiator of vanadium-evoked glucose metabolism in vitro and in vivo. *Journal of Biological Chemistry* **274**: 26617-26624.

95. Zorzano, A., M. Palacín, L. Marti, and S. García-Vicente. 2009. Arylalkylamine vanadium salts as new anti-diabetic compounds. *Journal of Inorganic Biochemistry* **103**: 559-566.

96. Liboiron, B. D., K. H. Thompson, G. R. Hanson, E. Lam, N. Aebischer, and C. Orvig. 2005. New insights into the interactions of serum proteins with bis(maltolato)oxovanadium(IV): Transport and biotransformation of insulin-enhancing vanadium pharmaceuticals. *Journal of the American Chemical Society* **127**: 5104-5115.

97. Willsky, G. R., A. B. Goldfine, P. J. Kostyniak, J. H. McNeill, L. Q. Yang, H. R. Khan, and D. C. Crans. 2001. Effect of vanadium(IV) compounds in the treatment of diabetes: in vivo and in vitro studies with vanadyl sulfate and bis(maltolato)oxovandium(IV). *Journal of Inorganic Biochemistry* **85**: 33-42.

98. Tang, S., B. Lu, and I. G. Fantus. 1998. Stimulation of I-125-transferrin binding and Fe-59 uptake in rat adipocytes by vanadate: Treatment time determines apparent tissue sensitivity. *Metabolism-Clinical and Experimental* **47**: 630-636.

99. Singer, S. J., and G. L. Nicolson. 1972. The fluid mosaic model of the structure of cell membranes. Cell membranes are viewed as two-dimensional solutions of oriented globular proteins and lipids. *Science* **175**: 720-731.

100. Day, C., and A. Kenworthy. 2009. Tracking microdomain dynamics in cell membranes. *Biochim Biophys Acta.* **1788**: 245-253.

101. Jacobson, K., O. G. Mouritsen, and R. G. Anderson. 2007. Lipid rafts: at a crossroad between cell biology and physics. *Nat Cell Biol* **9**: 7-14.

102. Brown, D. A., and E. London. 1998. Structure and origin of ordered lipid domains in biological membranes. *Journal of Membrane Biology* **164**: 103-114.

103. Lingwood, D., and K. Simons. 2010. Lipid rafts as a membrane-organizing principle. *Science* **327**: 46-50.

104. Edidin, M. 2003. The state of lipid rafts: from model membranes to cells. *Annual Review of Biophysics and Biomolecular Structure* **32**: 257-283.

105. Ilangumaran, S., and D. C. Hoessli. 1998. Effects of cholesterol depletion by cyclodextrin on the sphingolipid microdomains of the plasma membrane. *Biochemistry Journal* **335**: 433-440.

106. Harder, T., and K. Simons. 1997. Caveolae, DIGs, and the dynamics of sphingolipid-cholesterol microdomains. *Current Opinion in Cell Biology* **9**: 534-542.

107. Xiao, Z., and P. N. Devreotes. 1997. Identification of detergent-resistant plasma membrane microdomains in dictyostelium: enrichment of signal transduction proteins. *Molecular Biology of the Cell* **8**: 855-869.

108. Vainio, S., S. Heino, J.-E. Mansson, P. Fredman, E. Kuismanen, O. Vaarala, and E. Ikonen. 2002. Dynamic association of human insulin receptor with lipid rafts in cells lacking caveolae. *EMBO reports* **31**: 95-100.

109. Parpal, S., M. Karlsson, H. Thorn, and P. Stralfors. 2001. Cholesterol depletion disrupts caveolae and insulin receptor signaling for metabolic control via insulin receptor substrate-1, but not for mitogen-activated protein kinase control. *Journal of Biological Chemistry* **276**: 9670-9678.

110. Müller, G., A. Schultz, S. Wied, and W. Frick. 2005. Regulation of lipid raft proteins by glimeperide- and insulin-induced glycosylphosphatidylinositol-specific phospholipase C in rat adipocytes. *Biochemical Pharmacology.* **69**: 761-780.

111. Muller, G., and K. Geisen. 1996. Characterization of the molecular mode of action of the sulfonylurea, glimepiride, at adipocytes. *Hormone & Metabolic Research.* **28**: 469-487.

112. Panten, U., M. Schwanstecher, and C. Schwanstecher. 1996. Sulfonylurea receptors and mechanism of sulfonylurea action. *Experimental & Clinical Endocrinology & Diabetes.* **104**: 1-9.

113. Chamberlain, L. H., and G. W. Gould. 2002. The Vesicle- and Target-SNARE Proteins That Mediate Glut4 Vesicle Fusion Are Localized in Detergent-insoluble Lipid Rafts Present on Distinct Intracellular Membranes. *Journal of Biological Chemistry* **277**: 49750-49754.

114. Watson, R. T., S. Shigematsu, S.-H. Chiang, S. Mora, M. Kanzaki, I. G. Macara, A. R. Saltiel, and J. E. Pessin. 2001. Lipid raft microdomain compartmentalization of TC10 is required for insulin signaling and GLUT4 translocation. *The Journal of Cell Biology* **154**: 829-840.

115. Foran, P., L. Fletcher, P. Oaty, N. Mohammed, J. Dolly, and J. Tavarè. 1999. Protein kinase B stimulates the translocation of GLUT4 but not GLUT1 or transferrin receptors in 3T3-L1 adipoytes by a pathway involving SNAP-23, synaptobrevin-2, and/or cellubrevin. *The Journal of Biological Chemistry* **247**: 28087-28095.

116. Shechter, Y., A. Shanzer, and J. Libman. 1994. Vanadyl Complexes of Hydroxamate chelators and pharmaceutical compositions comprising them. *In* United States Patent. Yeda Research and Development Co. Ltd., Rehovot, Israel, U.S.A.

117. Stover, J., C. D. Rithner, R. A. Inafuku, D. C. Crans, and N. E. Levinger. 2005. Interaction of dipicolinatodioxovanadium(V) with polyatomic cations and surfaces in reverse micelles. *Langmuir* **21**: 6250-6258.

118. Aureliano, M., F. Henao, T. Tiago, R. O. Duarte, J. J. G. Moura, B. Baruah, and D. C. Crans. 2008. Sarcoplasmic reticulum calcium ATPase is inhibited by organic vanadium coordination compounds: Pyridine-2,6-dicarboxylatodioxovandium(V), BMOV, and an amavadine analogue. *Inorganic Chemistry* **47**: 5677-5684.

119. Crans, D. C., C. D. Rithner, B. Baruah, B. L. Gourley, and N. E. Levinger. 2006. Molecular probe location in reverse micelles determined by NMR dipolar interactions. *Journal of the American Chemical Society* **128**: 4437-4445.

120. Crans, D. C., A. M. Trujillo, S. Bonetti, C. D. Rithner, B. Baruah, and N. E. Levinger. 2008. Penetration of Negatively Charged Lipid Interfaces by the Doubly Deprotonated Dipicolinate. *Journal of Organic Chemistry* **73**: 9633-9640.

121. Crans, D. C., B. Baruah, A. Ross, and N. E. Levinger. 2009. Impact of confinement and interfaces on coordination chemistry: using oxovanadate reactions and proton transfer reactions as probes in reverse micelles. *Coordination Chemistry Reviews* **253**: 2178-2185.

122. Noblia, P., E. J. Baran, L. Otero, P. Draper, H. Cerecetto, M. Gonzalez, O. E. Piro, E. E. Castellano, T. Inohara, Y. Adachi, H. Sakurai, and D. Gambino. 2004. New Vanadium(V) Complexes with Salicylaldehyde Semicarbazone Derivatives: Synthesis, Characterization, and in vitro Insulin-Mimetic Activity - Crystal Structure of [VVO2(salicylaldehyde semicarbazone)]. *European Journal of Inorganic Chemistry*: 322-328.

123. Boron, W. F., and E. M. Boulpaep. 2003. Functional Organization of the Cell. *In* Medical Physiology: Updated Edition. W. R. Schmitt, editor. Elsevier Saunders, Philadelphia. 28.

124. Sakurai, H., K. Fujii, H. Watanabe, and H. Tamura. 1995. Orally-Active and Long-Term Acting Insulin-Mimetic Vanadyl Complex - Bis(Picolinato)Oxovanadium(Iv). *Biochemical and Biophysical Research Communications* **214**: 1095-1101.

125. McLauchlan, C. C., J. D. Hooker, M. A. Jones, Z. Dymon, E. A. Backhus, M. A. Youkhana, and L. M. Manus. 2010. Inhibition of acid, alkaline, and tyrosine (PTP1B) phosphatases by novel vanadium complexes. *Journal of Inorganic Biochemistry* **104**: 274-281.

126. Gao, X. L., L. P. Lu, M. L. Zhu, C. X. Yuan, J. F. Ma, and X. Q. Fu. 2009. Inhibitory Activities of Some Oxovanadium Complexes with N-Heterocyclic Ligands against PTP1B/ALP. *Acta Chimica Sinica* **67**: 929-936.

127. Yuan, C. X., L. P. Lu, X. L. Gao, Y. B. Wu, M. L. Guo, Y. Li, X. Q. Fu, and M. L. Zhu. 2009. Ternary oxovanadium(IV) complexes of ONO-donor Schiff base and polypyridyl derivatives as protein tyrosine phosphatase inhibitors: synthesis, characterization, and biological activities. *Journal of Biological Inorganic Chemistry* **14**: 841-851.

128. Roess, D. A., S. M. L. Smith, P. Winter, J. Zhou, P. Dou, B. Baruah, A. M. Trujillo, N. E. Levinger, X. Yang, B. G. Barisas, and D. C. Crans. 2008. Effects of

Vanadium-Containing Compounds on Membrane Lipids and on Microdomains Used in Receptor-Mediated Signaling. *Chemistry & Biodiversity* **5**: 1558-1570.

129. Yuen, V. G., C. Orvig, and J. H. McNeill. 1997. Effects of bis(maltolato)oxovanadium(IV) are distinct from food restriction in STZ-diabetic rats. *American Journal of Physiology-Endocrinology and Metabolism* **35**: E30-E35.

130. Yuen, V. G., P. Caravan, L. Gelmini, N. Glover, J. H. McNeill, I. A. Setyawati, Y. Zhou, and C. Orvig. 1997. Glucose-Lowering Properties of Vanadium Compounds: Comparison of Coordination Complexes with Maltol or Kojic Acid as Ligands. *Journal of Inorganic Biochemistry*: 109-116.

131. Vermathen, M., P. Vermathen, U. Simonis, and P. Bigler. 2008. Time-Dependent Interactions of the Two Porphyrinic Compounds Chlorin e6 and Mono-L-aspartyl-chlorin e6 with Phospholipid Vesicles Probed by NMR Spectroscopy. *Langmuir* **24**: 12521-12533.

132. Choi, S. Y., S. G. Oh, and J. S. Lee. 2001. Effects of lidocaine-HCl salt and benzocaine on the expansion of lipid monolayers employed as bio-mimicking cell membrane. *Colloids and Surfaces B-Biointerfaces* **20**: 239-244.

133. Vermathen, M., P. Stiles, S. J. Bachofer, and U. Simonis. 2002. Investigations of Monofluoro-Substituted Benzoates at the Tetradecytrimethylammonium Micellar interface. *Langmuir* **18**: 1030-1042.

134. Giustini, M., G. Palazzo, G. Colafemmina, M. D. Monica, M. Giomini, and A. Ceglie. 1996. Microstructure and Dynamics of the Water-in-Oil CTAB/n-Pentanol/n-Hexane/Water Microemulsion: A Spectroscopic and Conductivity Study. *Journal of Physical Chemistry* **100**: 3190-3198.

135. Caravan, P., L. Gemini, N. Glover, F. G. Herring, H. Li, J. H. McNeill, S. J. Rettig, I. A. Setyawati, E. Shuter, Y. Sun, A. S. Tracey, V. G. Yuen, and C. Orvig. 1995. Reaction chemistry of BMOV, bis(maltolato)oxovanadium(IV) - A potent insulin mimetic agent. *J. Am. Chem. Soc.* **117**: 12759-12770.

136. Ekwall, P., L. Mandell, and K. Fontell. 1969. The cetyltrimethylammonium bromide-hexanol-water system. *Journal of Colloid and Interface Science* **29**: 639-646.

137. Rodenas, E., and M. Valiente. 1992. The determination of some physical properties of reverse CTAB micelles in 1-hexanol. *Colloids and Surface* **62**: 289-295.

138. Vautier-Giongo, C., and B. L. Bales. 2003. Estimate of the Ionization Degree of Ionic Micelles based on Krafft Temperature Measurements. *Journal of Physical Chemistry B* **107**: 5398-5403.

139. Elvingson, K., A. G. Baro, and L. Pettersson. 1996. Speciation in Vanadium Bioinorganic Systems. 2. An NMR, ESR, and Potentiometric Study of the Aqueous H+-Vanadate-Maltol System. *Inorganic Chemistry* **35**: 3388-3393.

140. Cui, X., S. Mao, M. Liu, H. Yuan, and Y. Du. 2008. Mechanism of Surfactant Micelle Formation. *Langmuir* **24**: 10771-10775.

141. Behera, G. B., B. K. Mishra, P. K. Behera, and M. Panda. 1999. Fluorescent probes for structural and distance effect studies in micelles, reverse micelles and microemulsions. *Advances in Colloid and Interface Science* **82**: 1-42.

142. Rico, I., and A. Lattes. 1986. Formamide, a Water Substitute. 12. Krafft Temperature and Micelle Formation of Ionic Surfactants in Formamide. *Journal of Physical Chemistry* **90**: 5870-5872.

143. Szakacs, Z., M. Kraszni, and B. Noszal. 2004. Determination of microscopic acid-base parameters from NMR-pH titrations. *Analytical and Bioanalytical Chemistry* **378**: 1428-1448.

144. Peters, K., M. Davis, B. Howard, M. Pokross, V. Rastogi, C. Diven, K.Greis, E. Eby-Wilkens, M. Maier, A. Evdokimov, S. Soper, F. Genbauffe. 2003. Mechanism of insulin sensitization by BMOV (bis maltolato oxovanadium); inliganded vanadium (VO_4) as the active component. *Journal of Inorganic Biochemistry* **96**: 321-330.